Analysis of infiltration tests and performed in the Claduegne catchment in May-June 2012, contribution to WP3.4 of the FloodScale 2012-2015 ANR Project

Isabelle Braud, J.P. Vandervaere

HAL Id: hal-02602351

https://hal.inrae.fr/hal-02602351v1

Submitted on 16 May 2020

Analysis of infiltration tests performed in the Claduègne catchment in May-June 2012

Auteur : Isabelle Braud (Irstea, Lyon-Villeurbanne), Jean-Pierre Vandervaere (LTHE, Grenoble)

Diffusion du document : Participants FloodScale et HyMeX data base

Table of content

List of figures

List of tables

Abstract

In this report, we present the infiltration field campaign conducted in May-June 2012 in the 48 km^2 Claduègne catchment (Ardèche, France). First we present the different measurement protocols using either simple ring infiltrometers (*Beerkan* method) or suction disk infiltrometers. Then the sampling strategy is presented.

The theoretical aspects of infiltration equations and different methods used in infiltration tests analysis are described in details. In particular, the BEST (*Beerkan* Estimation of Soil Transfer) method is used in the analysis of single ring infiltration data and mini-disk infiltrometer with a -20 mm suction. This method is compared to the differential linear, single (DL-ST) method, showing reasonable agreement, although systematic biases are evidenced. Multiple suction disk infiltrometers are analyzed using permanent regime equations.

The single ring infiltration tests provide estimates of the retention curve and hydraulic conductivity curves. The infiltrometers provide information about the hydraulic conductivity close to saturation. We present the statistical analysis of the results, which show that the soils have generally high hydraulic conductivity, especially in forested soils. Dry bulk density is also much lower in natural soils than in cultivated soils. In situ measurements are compared with three representative pedo-transfer functions showing poor capability of the latter in reproducing observations. On the other hand, land use is found more discriminant in determining soil hydraulic properties. The statistical analysis of the samples allows defining two classes for dry bulk density with significantly different values gathering respectively natural and cultivated soils. In terms of saturated hydraulic conductivity, two land uses classes gathering forested fields and moors on the one hand, and pasture and cultivated land on the other hand can be distinguished. This allows proposing a first strategy of soil hydraulic properties spatialization in the Claduègne catchment, by combining the dry bulk density and hydraulic conductivity classes in three main families of soil hydraulic properties, depending on land use.

Acknowledgements

This report describes the experimental methods used to perform infiltration tests in the Claduègne catchment (Ardèche, France) in May-June 2012, the sampling protocols and the methods used for the infiltration tests analysis. It provides a first view of the obtained results.

1. General objectives of the study

This study is part of the FloodScale[1] project (Braud et al., 2014), dedicated to the observation and understanding of processes leading to flash floods in the Mediterranean context. More specifically, the study contributes to WP3.4 "Documentation and mapping of soil hydraulic properties, soil geometry and vegetation cover of small catchments".

Indeed, in infiltration-excess prone areas, the saturated hydraulic conductivity is the key factor, which must be documented. The working hypothesis is that the pedology/texture/land use combination is more relevant for the spatialization of soil hydraulic properties than the traditional pedo-transfer functions based on texture and dry bulk density only (Gonzalez-Sosa et al., 2010; Calianno, 2010; Rault, 2010). In particular, we would like to document the impact of macropores in enhancing hydraulic conductivity close to saturation (e.g. Schwartz et al., 2003; Gonzalez-Sosa et al., 2010).

The study was conducted at the scale of a small to medium size catchment which is part of the FloodScale pilot site: the Claduègne catchment (48 km^2), located in the Ardèche catchment. An infiltration test campaign was conducted in May-June 2012 to document the surface soil hydraulic properties using suction infiltrometers and positive head infiltration tests following the protocols proposed in Gonzalez-Sosa et al. (2010). Infiltration tests, using infiltrometers with multiple suctions were also performed at some locations.

This document presents the experimental protocols, the sampling strategy, as well as the methods used in the infiltration tests analysis. An analysis of the results is also conducted in order to assess the validity of the working hypothesis (largest impact of land use than soil texture on soil hydraulic properties) and to provide first recommendations for the spatialization of the surface soil hydraulic properties at the scale of the small catchments.

2. Protocols for infiltration tests

Two types of infiltration tests have been conducted:
- Infiltration tests based on suction-disk infiltrometers
- Infiltration tests with a positive head using the *Beerkan* method (Braud et al., 2005)

2.1. Protocol for suction-disk infiltrometers

Several types of infiltrometers were available in the various research teams
- Mini-disk infiltrometers (Sols Mesures with two diameters 4.5 and 8 cm) at Irstea-Lyon Villeurbanne (Figure 2-1a)
- Infiltrometers where the disk was removed from the tower (model SW 080 B, SDEC) available at HSM (Figure 2-1b)
- Infiltrometers according to Perroux and White (1988) at LTHE (Figure 2-1c)

---

[1] http://floodscale.irstea.fr/front-page-en?set_language=en

Figure 2-1 : (a) Photo of mini-disk infiltrometers (4.5 et 8 cm in diameter) (Photo Irstea) ; (b) Infiltrometer where the disk was removed from the tower from HSM (Photo C. Bouvier) ; (c) Infiltrometer used at LTHE (Photo I. Braud)

2.1.1. Field equipment

In addition to the infiltrometers presented above, the following equipment are required:
- GPS for getting the location of the infiltration test
- Chronometer (accuracy 1 s)
- Plastic can of about 20-30 l of water
- An installation template with the same size as the infiltrometer
- A flattening tool to get the surface plane, which can enter this template
- Contact sand with grains as small as possible (Fontainebleau sand type with diameter 0.1/0.35 mm ; Hostun sand, diameter 150 µm used at LTHE)
- Small cans for taking soil samples in order to get the initial soil moisture. If the cylinder volume is also known, it is possible to get the dry bulk density. At Irstea, we used cylinders with $\varnothing$ 4.3 cm and 2.5 cm height.
- One cylinder of known volume for taking a soil sample in order to determine the dry bulk density. At Irstea, we used cylinders with $\varnothing$ 7.5 cm and 5 cm height. The dry bulk density is generally lower with the smaller cylinder as it samples more superficial layers. The accuracy of the dry bulk density is generally higher with the 5 cm height cylinder.
- Plastic bags for taking soil samples (type freezing bags) used to get the particle size distribution
- Auger for taking soil samples

2.1.2. Measurement protocol

- Give a reference name to the infiltation test (field n°/test n°)
- Take the position of the location using the GPS
- Take off the vegetation and surface litter at the surface using a brush
- Put a sand layer ensuring a good contact between the soil and the infiltrometer (Figure 2-2a). This sand layer must not extend beyond the cylinder (see recommendation in Vandervaere, 1995, p.32-33[2] and a bad example in Figure 2-2b). The thickness of this

---

[2] « Cette couche [de sable] est aplanie au moyen d'une taloche. Le sable en excès dépassant la taille du disque doit impérativement être éliminée (en général juste après le début de l'essai) pour ne pas biaiser les résultats en

layer is discussed: at Irstea, we generally use the smallest thickness allowing getting a plane surface. At HSM a 1 cm thickness layer is used. This thickness is probably not critical when the permanent regime is analyzed, but is more important when transitory regime is also considered in the analysis.

- Take a soil sample (500 g to 1 kg) and put it in the plastic bag for particle size distribution analysis
- In a small can, take a soil sample (30 g) close to the infiltration site. Close the can, put a number. It will provide the initial soil moisture after 48 h soil drying in an oven at 105°C.
- Fill the infiltrometer with water and choose the suction. In case of multi-suction infiltration tests, start with the lowest pressure and increase it to gradually approach saturation. It is possible to test the tightness of the infiltrometer by closing the air entry: the water must not go out.
- Note the initial level in the infiltrometer on the field sheet
- Start the infiltration test with very close readings. The field sheet of JP Vandervaere proposes 5, 10, 15, 20, 30 s. But if the infiltration is very rapid, it can be more convenient that one person provides the ruler readings to the operator with the chronometer who takes the corresponding times.
- According to the infiltration speed, take a reading every 3 or 5 minutes.
- If only one pressure is considered, take off the infiltrometer once the permanent regime has been apparently reached and take a soil sample in the wet surface to get the final soil moisture and the dry bulk density (use the largest cylinder of known volume). If several suctions are monitored, set the next suction and continue the infiltration test without moving the infiltrometer from the surface.
- Perform three infiltration test per field sampling, if necessary at several levels along the slope
- If a multiple suction infiltration test is conducted, the recommended pressures are -150, -100, -60, -25, -10 and -5 mm.

Figure 2-2: Setting up the sand layer. On the left, a layer of several mm thickness. On the right, a minimum thickness layer, but which probably extends too much beyond the cylinder.

augmentant le rayon effectif à la surface du sol. Pour pallier ce risque, on peut utiliser un gabarit constitué d'un anneau de garde dont le diamètre intérieur est égal à celui du disque. Cet anneau, dans lequel la taloche peut être insérée, est simplement posé à la surface du sol et le sable, versé à l'intérieur »

2.2. Protocol for the Beerkan infiltration tests

"*Beerkan*" infiltration tests or "single ring infiltrometer" are realized using a positive water head value at the soil surface, using cylinders, laid over the surface (with a minimal burying to avoid lateral leaks).

They allow, when complemented with other *in situ* measurements (see below), the estimation of the parameters of the retention and hydraulic conductivity curves useful for water transfer modelling in the soil (with for example the Richards equation).

The theoretical bases of the method, as well as the practical use are described in Braud et al. (2005) and Lassabatère et al. (2006). The experimental protocol is adapted from Gonzalez-Sosa et al. (2010) for the cylinders of large diameters, which allow, when the spatial variability is important, to get more representative results, given the larger sampled surface.

For catchment scale modelling, it is recommended to select the files using topographical, land use and soil maps and to verify the accessibility of the sites. The sampled fields should have an area ranging between $10 \text{ m}^2 < S < 100 \text{ m}^2$. Three locations, distributed randomly within the field (or sampling different levels along a slope) are selected to perform three replicates. Each location must be geo-referenced. When the area is larger, it is convenient to realize one additional test per 100 m^2.

2.2.1. Field equipment

- GPS for getting the location of the infiltration test
- Cylinders of 400 mm x 250 mm, slightly cutting at the bottom
- Hammers (about 1 kg)
- Something allowing to hit on the cylinder in order to bury it as homogeneously as possible (like wooden beams)
- Metallic rulers of about 20-30 cm with 1mm accuracy
- Chronometer (accuracy 1 s)
- Plastic can of about 20-30 l of water
- Graduated buckets to measure the required water volume poured into the cylinder
- Thermometer
- Small cans for taking soil samples in order to get the initial soil moisture. If the cylinder volume is also known, it is possible to get the dry bulk density. At Irstea, we used cylinders with $\varnothing$ 4.3 cm and 2.5 cm height.
- One cylinder of known volume for taking a soil sample in order to determine the dry bulk density. At Irstea, we used cylinders with $\varnothing$ 7.5 cm and 5 cm height. The dry bulk density is generally lower with the smaller cylinder as it samples more superficial layers. The accuracy on the dry bulk density is generally higher with the 5 cm height cylinder.
- One square meter of plastic sheet
- Plastic bags for taking soil samples (type freezing bags) used to get the particle size distribution
- Auger for taking soil samples

2.2.2. Measurement protocol

- Give a reference name to the infiltration test (field n°/test n°)
- Take the position of the location using the GPS

- Take off the vegetation and surface litter at the surface using a brush
- Take a soil sample (500 g to 1 kg) and put it in the plastic bag for particle size distribution analysis
- In a small can, take a soil sample (30 g) close to the infiltration site (Figure 2-3a). Close the can, put a number. It will provide the initial soil moisture after 48 h soil drying in an oven at 105°C.
- Insert carefully the cylinder into the soil in order to reduce the soil surface alteration by turning from right to left and from left to right
- Put the wooden beams above the cylinder and hit it uniformly until the cylinder is buried in the soil (2 cm depth)
- Put the plastic sheet within the cylinder so that the whole cylinder surface is covered
- Pour a known water volume in the cylinder (2 to 12 l according to the cylinder size) and pour it in the cylinder above the plastic sheet. During the infiltration campaign in the Claduègne a 12 l water volume was used (Figure 2-3b).
- Take the water temperature
- Take off the plastic sheet rapidly but carefully to avoid overflowing water outside the cylinder
- Measure the initial water level height and start the infiltration test with very close readings (Figure 2-3c). The field sheet of JP Vandervaere proposes 5, 10, 15, 20, 30 s. But if the infiltration is very rapid, it can be more convenient that one person provides the ruler readings to the operator with the chronometer who takes the corresponding times.
- According to the infiltration speed, take a reading every 3 or 5 minutes.
- Once all the water has infiltrated, take off the cylinder and take a soil sample in the wet surface to get the final soil moisture and the dry bulk density (use the largest cylinder of known volume).
- Perform three infiltration test per field sampling, if necessary at several levels along the slope
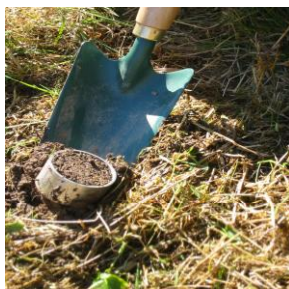
Figure 2-3: Photos of the Beerkan experimental protocol. Left: undisturbed soil sampling to get initial soil moisture and dry bulk density. Middle: Filling of the cylinder with the plastic sheet before starting the infiltration test. Right: Measurement of the water level during infiltration.

3. Sampling strategy

In order to test the working hypothesis (land use versus soil texture impact on soil hydraulic properties), the choosen sampled fields were selected in order to sample a maximum number of combinations of geology / pedology / land use.

The following GIS layers were used in the analysis (see details in Bonnet, 2012):

- A 25 m Digital Elevation Model (DTM) from BDTopo® IGN

- A pedology map from the Ardèche soil data base (Chambre d'Agriculture de l'Ardèche) from the IGCS[3] program with resolution 1/250 000.
- The geology map of the Auzon catchment from BRGM with resolution 1/25 000.
- The 2006 Corine Land Cover map from IFEN[4] with resolution 100 m
- The road network provided by BDTopo® IGN
- The land registry provided by BDTopo® IGN

It was also tried to include a map characterizing the likelihood of surface runoff to occur (Bonnet, 2012) in the analysis, but this was leading to a too large number of combinations.

By overlaying the geology / pedology and land use maps a series of potential fields of interest were selected, taking into account their accessibility. The first selection was composed of combination including two types of geology: basalt and limestones; five land use classes: vineyards, pasture, forest, herbaceous, crops; and seven soil cartographic units from the pedology map, leading to 37 potential field locations.

A field survey was conducted at the beginning of May to confirm if the identified potential fields were similar to what was expected. The main source of differences was related to land use as the analysis was conducted with the 2006 Corine Land Cover map and the land use had sometimes changed in the meantime (building, abandonment of crops, etc.). After this field survey, the land registry was used to identify the field owners, who were contacted to obtain their agreement/refusal for sampling their fields.

Finally, a set of 18 fields was sampled through two field campaigns conducted between May 23-25 and June 18-19 2012. Table 3-1 provides the main characteristics of the sampled fields and the number of infiltration tests conducted in those fields (*Beerkan*, mini-disk infiltrometer with one suction, infiltrometer sampling using multiple suctions – in this case the used suctions are indicated).

The location of the fields is provided in Figure 3-1, together with the whole FloodScale instrumentation within the Auzon catchment.

---

[3] http://www.gissol.fr/programme/igcs/igcs.php
[4] http://www.stats.environnement.developpement-durable.gouv.fr/clc/CORINE_Land_Cover_-_Saisie_Demande.jsp

Field n°	Land use	Geology	US	Score for sensitivity to runoff production	Beerkan	Mini-disk 4.5 + 8 cm	LTHE infiltrometer
3	Grassland (mowed alfafa)	Basalt	64	2	3	2+1	
5	Hedge of oaks	Basalt	64	2	3	0	
14	Natural grassland	Limestones	33	2	3	2+1	-9, -4, -1.5, -1, -0.5cm
16	Coniferous forest	Limestones	33	2	3	2+1	-10, -6, -4, -2, -0.7cm
17	Fallow land : moor and herbaceous	Limestones	33	3	3	2	
22	Grassland grazed by sheeps	Basalt	65	1	3	2	
25	Oak woods	Basalt	65	0	3	2+1	-7, -4, -2, -1, -0.5cm + -2cm
46	Grazed permanent pasture	Limestones	26	1	3	2	
46b	Ploughed vineyard	Limestones	26	1	3	1	
52	Oak woods	Limestones	29	2	4	2	
58	Natural grassland	Limestones	29	3	3	2	
60	Fallow land : moor and herbaceous	Limestones	29	2	3	2	
74a	Moved ray grass grassland	Limestones	8	2	3	2+1	-7, -4, -2, -1, -0.5cm
74b	Vineyard with herbaceous	Limestones	8	2	4	2+2	-7, -4, -3, -1, -0.5cm
74C	Grassland (mowed alfafa)	Limestones	8	2	3	2+2	
82b	Vineyard	Limestones	27	3	4	0	
82t	Grassland (mowed alfafa)	Limestones	27	3	3	3	

Table 3-1: Main characteristics of the sampled fields.

14
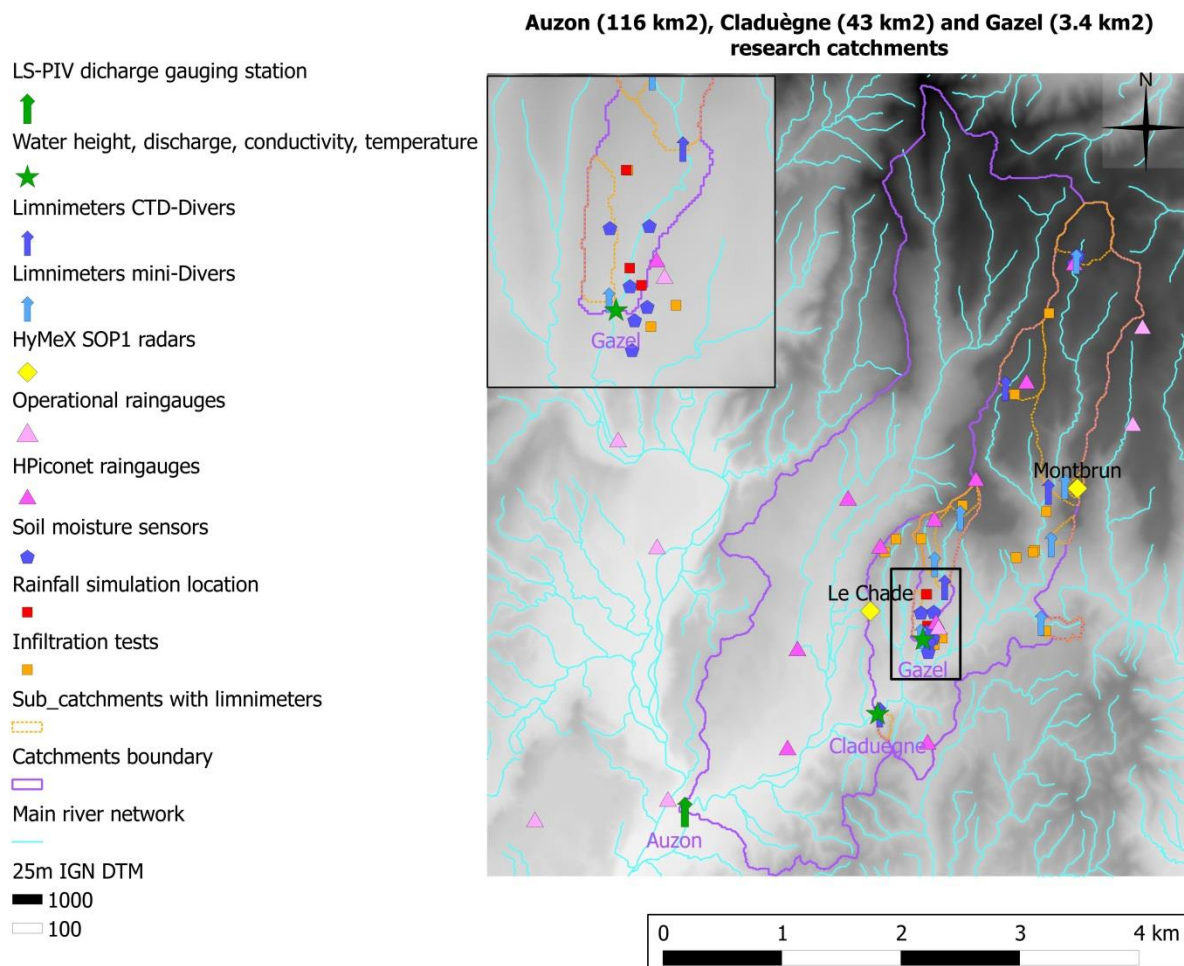
Figure 3-1: Instrumentation of the Auzon catchment. The location of the infiltration test is shown as orange squares (From Braud et al., 2014).

4. Analyses of the *Beerkan* and mini-disk infiltration tests

4.1. Theory of infiltration (permanent and transient regime)

The following description is taken from Gonzalez-Sosa and Braud (2009)

From the theory of infiltration proposed by Philip (1969), several methods have been proposed to estimate soil sorptivity and (near)-saturation hydraulic conductivity from disk infiltrometer data. The methods proposed by Zhang (1997), Vandervare et al. (2000a) and Smiles and Knight (1976) will be presented in this section. These methods are based on an approximation of the infiltration equation for short to medium time steps.

The axisymmetric infiltration equation (3D) can be described using the following approximation for transient flow, when the initial water content is such that the initial hydraulic conductivity is much smaller than the value corresponding to the pressure of the infiltrometer (Haverkamp et al., 1994).

$$I(t) = S\sqrt{t} + Dt \tag{1}$$

where I is the cumulative infiltration per unit of area (m), t is time (s), and S is the capillary sorptivity (m s$^{1/2}$) and D is given by:

$$D = \frac{2-\beta}{3}K + \frac{\phi S^2}{R(\theta_i - \theta_0)} \tag{2}$$

with β, a constant constrained to be $0<\beta<1$, R is the radius of the infiltrometer (m), θ_i is the initial water content and θ_0 is the final water content, and $\phi=0.75$ (Smettem et al., 1994). In the following, and in order to simplify notation, it will be assumed that $S = S(\theta_i, \theta_0)$

The introduction of the second right hand side term in Eq. (1) was necessary because the expression provided by the first right hand-side term is only valid for very short times, especially with axisymmetric infiltration. In practice, in the field, it was difficult to obtain enough data points of cumulative infiltration at short time steps for a reliable sorptivity estimation using only the short time approximation.

For simplicity, Eq. (1) is written as:

$$I(t) = C_1\sqrt{t} + C_2 t \tag{3}$$

with $\quad S = C_1 \tag{4}$

and $\quad C_2 = \frac{2-\beta}{3}K + \frac{\phi S^2}{R(\theta_i - \theta_0)} \tag{5}$

The sorptivity is obtained using the expression proposed by Parlange (1975):

$$S = S(\theta_i, \theta_0) = 2\int_{\theta_i}^{\theta_0}(\theta_0 + \theta - 2\theta_i)D(\theta)d\theta \tag{6}$$

where $D(\theta)$ is the hydraulic diffusivity (m^2 s^{-1})

The first method that was applied to obtain the sorptivity and hydraulic conductivity is the cumulative infiltration (CI) fitting proposed by Zhang (1997)
where

$$S(h_0) = \frac{C_1}{A_1}$$
(7)

$$K(h_0) = \frac{C_2}{A_2}$$
(8)

For soils with the van Genuchten (1980) type retention function, the coefficients have the empirical form

$$A_1 = \frac{1.4b^{0.5}(\theta_0 - \theta_i)^{0.25}\exp[3(n-1.9)\alpha h_0]}{(\alpha r_0)^{0.15}}$$
(9)

and

$$A_2 = \frac{11.65(n^{0.1} - 1)\exp[2.92(n-1.9)\alpha h_0]}{(\alpha r_0)^{0.91}} \qquad n \geq 1.9$$
(10)

$$A_2 = \frac{11.65(n^{0.1} - 1)\exp[7.5(n-1.9)\alpha h_0]}{(\alpha r_0)^{0.91}} \qquad n \leq 1.9$$
(11)

$\alpha = 1/h_{VG}$ and n are van Genuchten parameters, r_0 is the radius of the mini-disk infiltrometer, h_0 is the applied suction, θ_0 is the water content at h_0, θ_i is the initial water content, and b is a parameter, with a representative value equal to 0.55 (Warrick and Broadbridge, 1992).

The second method, (DL) differentiation linearization, was proposed by Vandervare et al. (2000a, b). It is described by:

$$\frac{dI}{d\sqrt{t}} = C_1 + 2C_2\sqrt{t}$$
(12)

where $\dfrac{dI}{d\sqrt{t}}$ is approximated by

$$\frac{dI}{d\sqrt{t}} \approx \frac{\Delta I}{\Delta\sqrt{t}} = \frac{I_{i+1.} - I_i}{\sqrt{t_{i+1}} - \sqrt{t_i}} \qquad (i=1, n_p-1)$$
(13)

where n_p is the number of data points, and the corresponding $\sqrt{t}$ is calculated as geometric mean

$$\sqrt{t} = [\sqrt{t_{i+1}t_i}]^{1/2} \qquad (i=1, n_p-1)$$
(14)

The third method is based on Smiles and Knight (1976) linear fitting (CL) (cumulative linearization). The solved equation is obtained by dividing both sides of Eq. (3) by $\sqrt{t}$

$$\frac{I(t)}{\sqrt{t}} = C_1 + C_2\sqrt{t} \tag{15}$$

The advantage of Eqs. (12) and (15) is that they lead to a linear fitting, which is more robust than a quadratic fitting when the fitting is directly performed using Eq. (3).

These three methods can be applied to estimate the soil sorptivity and hydraulic conductivity at pressure h_0, from a fitting of coefficients C_1 and C_2 in Eq. (3), (12) or (15). Then, sorptivity is directly equal to C_1 (Eq. [3]) and the conductivity is deduced from $C_2 = D$ by:

$$K = \frac{3}{2-\beta}\left[C_2 - \frac{\phi S^2}{R(\theta_i - \theta_0)}\right] \tag{16}$$
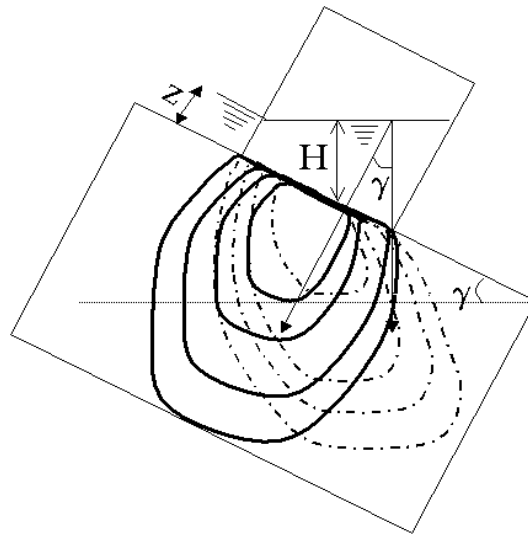
Figure 4-1: Scheme of water front when the surface has a non zero slope where z is water height perpendicular to the topsoil surface, H is the water height within the infiltrometer and γ is the topsoil surface slope.

The drawback of the methods that deduce hydraulic conductivity from Eq. (16) is that they can lead to negative values of the hydraulic conductivity which are not physical. However, this is also an advantage since it becomes the sign that the infiltration equation is not valid when another method will not provide negative values, thus leading to accept possible meaningless values. In fact, linearization methods are those that allow detecting validity problems of the infiltration equation; especially the DL method which eliminates the problem of the contact sand layer.

In the context of the experimental set up, the three methods are conditioned by the sand contact layer between the infiltrometer surface and the topsoil, organic matter content and sloping field surface. In our case the surface slope could affect the water flow and possibly also the measured infiltration.

According to Chen and Young (2006) vertical direction of the infiltration I_h on a sloping surface is evaluated by the relation (see Figure 4-1)

$$\frac{I_h(t,\gamma)}{I_h(t,0)} = \frac{1}{\cos\gamma} \tag{17}$$

This relationship establishes that the sloping surface increases the infiltration at small t by a factor of 1/cosγ which is the same result as the equation of Philip (1991), given the coordinate change. For $t \rightarrow \infty$, or for large infiltration depths, the saturated hydraulic conductivity can be approximated as

$$K_s t \approx I_h$$
(18)

In synthesis, the infiltration at short time is controlled by capillary forces, which would be independent of the slope angle for homogeneous and isotropic soils. However, increasing the slope angle increases the slope length, and increase the total infiltration volume. For large t (or large I), the controlling mechanism becomes the gravity, which would reduce the infiltration by a factor *cosγ*. This effect cancels with increasing slope length, and slope effect vanishes. Philip (1991) indicates that slope produces a maximum variation between horizontal and normal infiltration on sloping soil surface of about 13%. Variations are much smaller for small and moderate t values. The effect of slope was therefore neglected in subsequent analyses.

4.2. Analysis of permanent regimes

The following elements are translated from Vandervaere (1995) and correspond to the method used by HSM for the analysis of its infiltration tests, using permanent regime from infiltrometers.

Reynolds and Elrik (1991) and Ankeny et al. (1991) propose to determine the hydraulic conductivity from the Wooding (1968) solution, coupling fluxes obtained at the same location, using different water potential to determine K_0 and Φ_0.

Using the hypothesis of an exponential relationship between K and h (Gardner, 1958), the Kirchhoff potential has the following simple form:

$$\Phi_0 = \frac{K_0 - K_i}{\alpha}$$
(19)

where $K_i << K_0$ if the soil is initially dry enough. Wooding (1968) analysis for a value h_0 of the soil water pressure, leads to the following expression:

$$q_0 = K_s \exp(\alpha h_0)\left(1 + \frac{4}{\pi r \alpha}\right)$$
(20)

Or in a logarithmic form:

$$\ln q_0 = \ln\left\{K_s\left(1 + \frac{4}{\pi r \alpha}\right)\right\} + \alpha h_0$$
(21)

With $K_S = K_o exp(\alpha h_o)$
(22)

where the unknowns are K_s and α. Equations (19) et (22) finally lead to:

$$K_0 = \frac{\exp\left(\ln q_0 - \alpha h_0\right)}{1 + \dfrac{4}{\pi r \alpha}} \exp\left(\alpha h_0\right) \tag{23}$$

Reynolds and Elrick (1991) and Ankeny et al. (1991) propose to measure successively q_0 at two (or more) soil water pressures and to plot the (h_0, $\ln q_0$) couples in a graph. The slope of the straight line passing through two (or more) consecutive points leads to the α values, while the intercept at $h = 0$ given by:

$$Intercept = ln\left\{K_s\left(1 + \frac{4}{\pi r \alpha}\right)\right\} \tag{24}$$

allows the computation of K_s.

Practically, the successive *qi* values corresponding to values *hi* of the soil water pressure are obtained at the same location, which allows removing the effect of the spatial variability of soil properties. Soil water pressures values are applied in an increasing order, in order to avoid hysteresis impact. On the other hand, the method does not provide sorptivity values, as initial and final value of the soil water content cannot be measured for each infiltration step.

If Equation (21) is verified, successive points *lnqi-hi* should be located in a perfect straight line. However, in practice, this is seldom verified, which is equivalent to consider that α is a function of *h*, and that the *lnqi-hi* couples do not belong to a unique straight line. Reynolds and Elrick (1991) and Ankeny et al. (1991) propose that *K(h)* is considered as a piece-wise exponential function. For two values of the soil water pressure, *hi* and *hj (hi<hj)*, close enough to each other so that α can be considered to have a unique constant value αij in the interval $\Delta hij = [hi ; hj]$, Equation (21) can be written :

$$lnq_i = ln\left\{K_s\left(1 + \frac{4}{\pi r \alpha_{ij}}\right)\right\} + \alpha_{ij} h_i \tag{25a}$$

$$lnq_j = ln\left\{K_s\left(1 + \frac{4}{\pi r \alpha_{ij}}\right)\right\} + \alpha_{ij} h_j \tag{25b}$$

where *Kij* is a parameter having a physical meaning, only if *hj = 0*. In this case, *Kij* can be associated to *Ks*, the saturated hydraulic conductivity.

With this assumption, Equation (23) can be written:

$$K\left(h_m\right) = \frac{\exp\left[\ln q_i - \alpha_{ij}\left(h_m - h_i\right)\right]}{1 + \dfrac{4}{\pi r \alpha}} \tag{26}$$

with $h_m = \dfrac{h_i + h_j}{2}$

Given the hypotheses and, in particular the assumption that *K(h)* is a piece-wise exponential function, equations (25) and (26) are only valid in the Δ*hij* interval if the following equalities are true :

$$\frac{K_j}{K_i} = \frac{\Phi_j}{\Phi_i} = \frac{q_j}{q_i} = \exp\left(\alpha_{ij}\Delta h_{ij}\right)$$

(27)

Where the α*ij* coefficients are computed using:

$$\alpha_{ij} = \frac{\ln\left(\dfrac{q_j}{q_i}\right)}{\Delta h_{ij}}$$

(28)

The mathematical developments of Ankeny et al. (1991) introduce the following approximation:

$$\Phi\left(h_j\right) - \Phi\left(h_j\right) \approx \left[K\left(h_i\right) + K\left(h_j\right)\right]\frac{\Delta h_{ij}}{2}$$

(29)

which is equivalent to a linearisation of the Φ *(h)* function between *hi* and *hj*. The expression of α*ij* proposed by Reynolds and Elrick (1991):

$$\alpha_{ij} = \frac{\ln\left(\dfrac{K_j}{K_i}\right)}{\Delta h_{ij}}$$

(30)

is replaced with

$$\alpha_{ij} = \frac{2\left(K_j - K_i\right)}{\Delta h_{ij}\left(K_i + K_j\right)} = \frac{2\left(q_j - q_i\right)}{\Delta h_{ij}\left(q_i + q_j\right)}$$

(31)

Then, equation (20) becomes:

$$K_i = \frac{\pi r\left(q_j - q_i\right)}{\pi r\left(\dfrac{q_j}{q_i} - 1\right) + 2\left(\dfrac{q_j}{q_i} + 1\right)\left(h_j - h_i\right)}$$

(32)

which provides the value of the hydraulic conductivity for *hm*.

This method was used for the interpretation of the infiltrometer tests performed by LTHE (last column of Table 3-1).

4.3. Analysis of transient regimes using the method of Lassabatère et al. (2006)

The theoretical background of the BEST (*Beerkan* Estimation of Soil Transfer) method is described in Braud et al. (2005) and its practical implementation is reported in Lassabatère et al. (2006). We will refer to the method as the L06 method in the following. The following description borrows lots of material from these two references, as well as from the work of Gonzalez-Sosa et Braud (2009).

In this approach, the aim is to determine the retention curve $h(\theta)$, relating the soil water pressure h (m) to the soil volumetric water content θ (m³ m⁻³); and the hydraulic conductivity curve $K(\theta)$ relating the soil hydraulic conductivity K (m s⁻¹) to the soil water content. The retention curve is modeled using the Van Genuchten (1980) approach (Eq. (33)) and the hydraulic conductivity using the Brooks and Corey (1964) model (Eq. (35)).

$$\frac{\theta}{\theta_s} = \left\{ 1 + \left(\frac{h}{h_{VG}} \right)^n \right\}^{-m} \tag{33}$$

with
$$n = \frac{k}{1-m} \tag{34}$$

where θ_s is the saturated water content (m³ m⁻³), h_{VG} is a normalization parameter for the water pressure, m and n are shape parameters and k is an integer chosen to be 1 (Mualem, 1976) or 2 (Burdine, 1953). In the following $k=2$ was used.

$$K(\theta) = K_s \left(\frac{\theta}{\theta_s} \right)^\eta \tag{35}$$

where K_s (m s⁻¹) is the saturated hydraulic conductivity and η is a shape parameter related to m and n by:

$$\eta = \frac{2}{mn} + 2 + p \tag{36}$$

where p is a tortuosity parameter equal to 0 (Childs and Collis-George, 1950) or 1 (Mualem, 1976).

The objective is thus to derive, at each location, the values of the parameters of the retention and hydraulic conductivity curves, namely the shape parameters m, n and η and the structure parameters θ_s, h_{VG} and K_s.

Two steps can be distinguished in the L06 method. The first one corresponds to the estimation of the shape parameters m, n and η from soil texture. The second one is the optimisation of the infiltration tests in order to derive the structure parameters S, h_{VG} and K_s. In the following, it is assumed that θ$_s$ is available from field measurements, and, as mentioned before is assumed to be equal to the measured final water content.

Estimation of shape parameters
Soil texture is derived from the particle-size distribution (< 2 mm), determined from a disturbed soil sample, and giving a curve with at least five fractions (clay, fine silt, coarse silt, fine sand, coarse sand). As a general rule, the more fractions that are determined, and the better is the curve fitting. The particle-size data provide the cumulative frequency distribution, $F(d)$, as a function of particle diameter, d (m), to which the following curve is fitted

$$F(d) = \left\{ 1 + \left(\frac{d_g}{d} \right)^B \right\}^{-A} \qquad \text{with} \qquad A = 1 - \frac{2}{B} \tag{37}$$

where d_g (m), is the normalization parameter for the particle diameter, and A and B are the shape parameters of the curve. The quantities d_g and B are optimized by least squares techniques, stability of the convergence being achieved by using a change of variable $x=1/d$. The shape parameters m and n of the water retention curve can be derived from the knowledge of soil texture, and more specifically, from the knowledge of the A and B values. Following Haverkamp *et al.* (2005), we introduce soil specific shape indexes, p_A, for the particle-size distribution and, p_m, for the water retention curve given respectively by:

$$p_A = \frac{AB}{1+A} \tag{38}$$

and $\quad p_m = \frac{mn}{1+m} \tag{39}$

where mn and AB are the products of the shape parameters of the retention and cumulative particle-size curves, respectively. They are related through

$$p_A = (1+\kappa)p_m \tag{40}$$

where $\quad \kappa = \frac{2s-1}{2s(1-s)} \tag{41}$

and s is the solution of the non-linear equation below given by Fuentes et al. (1998):

$$(1-\varepsilon)^s + \varepsilon^{2s} = 1 \tag{42}$$

where ε is the soil porosity.

The derivation of the shape parameter for the hydraulic conductivity curve η is performed using the classical capillary model of Eq.(36). In the following, the chosen value for the tortuosity parameter is 1 (Mualem, 1976).

Shape parameters of the water retention and hydraulic conductivity curves can therefore be derived from sole knowledge of soil texture.

Optimisation of the infiltration test and estimation of sorptivity and hydraulic conductivity

The interpretation of infiltration tests using the L06 method starts from a more general infiltration equation than Eq.(1) and (2). Haverkamp et al. (1994) proposed an approximation of the full 3D infiltration equation for short to medium time steps, which reads:

$$I_{3D}(t) = S\sqrt{t} + \left[\frac{\phi S^2}{R(\theta_0 - \theta_i)} + K_i + \frac{2-\beta}{3}(K_0 - K_i) \right] t \tag{43}$$

where it is no more assumed that $K_i << K_0 = K(h_0)$

On the other hand, for long time steps, Haverkamp et al. (1994) show that the infiltration can be written (subscript ₃D is omitted in the following for simplicity):

$$I_\infty = \left[K_0 + \frac{\phi S^2}{R(\theta_0 - \theta_i)} \right] t + \frac{S^2}{2(K_0 - K_i)(1-\beta)} \ln\left(\frac{1}{\beta} \right) \tag{44}$$

which corresponds to a linear variation with time.

Contrarily to the methods presented in section 4.1, which only exploit the short time steps behavior of the infiltration, the L06 method tries to take into account both short and long time

steps behavior. The parameter estimation can thus be based on more data than the approaches presented in section 4.1.

For long time steps, the infiltration flux is given by the slope of the curve $I(t)$:

$$q_\propto = K_0 + \frac{\phi S^2}{R(\theta_0 - \theta_i)} = K_0 + A S^2 \tag{45}$$

with

$$A = \frac{\phi}{R(\theta_i - \theta_0)} \tag{46}$$

The intercept of Eq.(44) is given by:

$$b_\propto = C \frac{S^2}{K_0} \tag{47}$$

with

$$C = \frac{1}{2\left(1 - \frac{K_i}{K_0}\right)(1-\beta)} \ln\left(\frac{1}{\beta}\right) = \frac{1}{2(1-\beta)\left[1 + \left(\frac{\theta_i}{\theta_0}\right)^\eta\right]} \ln\left(\frac{1}{\beta}\right) \tag{48}$$

which uses Eq.(35) such that:

$$\frac{K_i}{K_0} = \left(\frac{\theta_i}{\theta_0}\right)^\eta \tag{49}$$

Data for large time steps are used to fit Eq.(44) and thus derive estimates of $q_\propto$ and $b_\propto$.

For the interpretation of infiltration data at short times steps, two methods were tested:

i) Method 1: The first method follows the recommendations of Lassabatère et al. (2006) and consists in introducing Eq. (45) within Eq.(43), so that the only unknown becomes the sorptivity. This ensures a higher robustness of the optimization algorithm.

$$I_{3D}(t) = S\sqrt{t} + \left[A(1-B)S^2 + Bq_\propto\right]t \tag{50}$$

with

$$B = \frac{K_i}{K_0} + \frac{2-\beta}{3}\left(1 - \frac{K_i}{K_0}\right) = \left(\frac{\theta_i}{\theta_0}\right)^\eta + \frac{2-\beta}{3}\left(1 - \left(\frac{\theta_i}{\theta_0}\right)^\eta\right) \tag{51}$$

ii) Method 2: The second method uses the intercept provided by Eq.(47) instead of the slope (Yilmaz et al., 2008). The latter is introduced within Eq.(43) and, once again, the expression only depends on the sorptivity, which can be optimized robustly.

$$I_{3D}(t) = S\sqrt{t} + \left[A + \frac{BC}{b_\propto}\right]S^2 t \tag{52}$$

The optimization is performed by minimizing the sum of square errors between the simulated (using either Eq.(50) or (52)) and the measurements using k measured values, k being varied successively from 5 to n_p, the number of measurement points. The objective function is written:

$$f(S^2, k) = \sum_{i=1}^{k}\left[I_{exp}(t_i) - I(t_i)\right]^2 \tag{53}$$

where t_i, $I(t_i)$ are the measured values of infiltration as a function of time.

The optimization can also be performed using the infiltration flux data, where the infiltration flux is calculated as proposed by Lassabatère et al. (2006) (see their Eq. [18b]). Both methods were used in the following analysis.

The approximation provided by Eq.(43) is only valid for times t_i lower than the gravity time t_{grav}, which corresponds to the time at which gravity begins to dominate the flow process (Philip, 1969):

$$t_{grav} = \left(\frac{S}{K_0}\right)^2 \tag{54}$$

Practically, Eq.(53) is optimized by varying k for about 5 to n_p and when the time is larger than t_{grav}, i.e. for $k=p_I$, the equation is no more valid. The value of the optimized parameter S^2 for $k=p_I$ is thus the retained value.

Note that the data for $k> p_I$ are not lost, as they are used to fit Eq.(44) for longer times. In the interpretation of the infiltration test, it means that Eq.(43) is valid for k smaller than p_I. Then Eq.(44) is valid.

The optimization process provides an estimate of the sorptivity S^2. Then, an estimate of the hydraulic conductivity can be obtained using Eq.(45) (method 1) or Eq.(47) (method 2):

$$K_0 = q_\infty - AS^2 \tag{55}$$

$$K_0 = C\frac{S^2}{b_\infty} \tag{56}$$

Note that, up to this step, the method can be applied both for infiltration test under suction or with a positive head. Thus it can be used for the interpretation of **both the mini-disk and single ring infiltration tests**.

As the saturated water content is estimated from the final and dry bulk density measurements, the last parameter which must be estimated to get all the parameters needed for the retention and hydraulic conductivity curves (Eqs. (33) and (35)) is the normalization parameter for the water pressure h_{VG}. This is achieved using the definition of the sorptivity provided in Eq.(6). The sorptivity can be rewritten as (Braud et al., 2005):

$$S(\theta_i,\theta_0) = \underbrace{S(0,\theta_s)}_{1}\underbrace{\frac{S(\theta_i,\theta_s)}{S(0,\theta_s)}}_{2}\underbrace{\frac{S_1(\theta_i,\theta_0)}{S_1(\theta_i,\theta_s)}}_{3}, \tag{57}$$

where the significance of the various terms is as follows.

1. The first term represents the integral given by Eq.(6) from 0 to θ_s, i.e. over the whole range of possible soil moisture content. It does not depend on initial and boundary conditions and can be considered as an integral soil characteristic.
2. The second term represents the influence of initial conditions.
3. The third term represents the influence of boundary conditions. When the surface head is positive, this term reduces to unity.

The first term of Eq.(57) can be calculated analytically for the combination of the van Genuchten retention model and the Brooks and Corey hydraulic conductivity model. This leads to:

$$S^2(0,\theta_s) = -c_{p\_VG}K_s\theta_s h_{VG}, \tag{58}$$

where c_p is a texture only dependent factor, the expression for which is given by Haverkamp *et al.* (1998):

$$c_{\mathrm{p\_VG}} = \Gamma\left(1 + \frac{1}{n}\right)\left\{\frac{\Gamma\left(m\eta - \frac{1}{n}\right)}{\Gamma(m\eta)} + \frac{\Gamma\left(m\eta + m - \frac{1}{n}\right)}{\Gamma(m\eta + m)}\right\}, \tag{59}$$

where Γ is the classical Gamma function.

Braud et al. (2005) propose an equation for estimating the sorptivity $S(\theta_i, \theta_s)$, which remains sufficiently accurate for the range $\theta_0/\theta_s < 0.8$ for sand and <0.9 for clay

$$S(\theta_i, \theta_s) = S(0, \theta_s)\frac{\theta_s - \theta_i}{\theta_s}\frac{K_s - K_i}{K_s}. \tag{60}$$

Thus, when the surface head is positive or zero, the final water content is equal to the saturated water content ($\theta_0 = \theta_s$) and Eq. (57) reduces to the first two terms. An estimate of h_{VG} can be deduced as:

$$h_{VG} = -\frac{S^2}{c_{p\_VG}(\theta_s - \theta_i)K_s\left[1 - \left(\frac{\theta_i}{\theta_s}\right)^\eta\right]} \tag{61}$$

When the surface head is negative as in the case of mini-disk infiltration test, we have no estimate of the third term of Eq. (57) and thus the infiltration test can no more be used to derive an estimate of h_{VG}. However by estimating the water content corresponding to $h=h_0$ using Eq.(33), it will be possible to verify if the hydraulic conductivity derived from the mini-disk fits the hydraulic conductivity curve given by Eq.(35).

It is also possible to obtain an estimate of the hydraulically active pore radius λm, the expression of which can be found in Angulo-Jaramillo et al. (1996) and is derived from results of White and Sully (1987):

$$\lambda_m = \frac{\sigma}{\rho_w g}\frac{(\theta_0 - \theta_i)(K_0 - K_i)}{bS^2} \tag{62}$$

where $\sigma=73\ 10^{-3}$ N m^{-1} is the surface tension, $\rho w=1000$ kg m^{-3} is the water volumetric mass, $g=9.81$ m s^{-2} is the acceleration of gravity, b is a constant generally taken to be 0.55.

The L06 method was used for the interpretation of the *Beerkan* and mini- infiltrometer tests performed by Irstea (first columns of Table 4).

4.4. Analysis of transient regimes using the Differential Linearization (DL-ST) method

The differentiation linearization (DL) , was proposed by Vandervare et al. (2000a, b). It is described by:

$$\frac{dI}{d\sqrt{t}} = C_1 + 2C_2\sqrt{t} \tag{63}$$

In Vandervaere et al. (2000a) it is proposed to approximate $\dfrac{dI}{d\sqrt{t}}$ by

$$\frac{dI}{d\sqrt{t}} \approx \frac{\Delta I}{\Delta \sqrt{t}} = \frac{I_{i+1.} - I_i}{\sqrt{t_{i+1}} - \sqrt{t_i}} \qquad (i=1, n_p\text{-}1) \tag{64}$$

where n_p is the number of data points, and the corresponding $\sqrt{t}$ is calculated as geometric mean

$$\sqrt{t} = [\sqrt{t_{i+1}t_i}]^{1/2} \quad (i=1, n_p\text{-}1) \tag{65}$$

However, if we assume that Eq. (3) is valid, we can write Eq. (63) as follows:

$$\frac{I_{i+1} - I_i}{\sqrt{t_{i+1}} - \sqrt{t_i}} = \frac{1}{\left(\sqrt{t_{i+1}} - \sqrt{t_i}\right)}\left[C_1\left(\sqrt{t_{i+1}} - \sqrt{t_i}\right) + C_2\left(t_{i+1} - t_i\right)\right]$$

$$\frac{I_{i+1} - I_i}{\sqrt{t_{i+1}} - \sqrt{t_i}} = C_1 + C_2 \frac{\left(\sqrt{t_{i+1}} + \sqrt{t_i}\right)\left(\sqrt{t_{i+1}} - \sqrt{t_i}\right)}{\left(\sqrt{t_{i+1}} - \sqrt{t_i}\right)}$$

$$\frac{I_{i+1} - I_i}{\sqrt{t_{i+1}} - \sqrt{t_i}} = C_1 + 2C_2\left(\frac{\sqrt{t_{i+1}} + \sqrt{t_i}}{2}\right) = C_1 + 2C_2 t_i^* \tag{66}$$

where

$$t_i^* = \left(\frac{\sqrt{t_{i+1}} + \sqrt{t_i}}{2}\right) \tag{67}$$

The derivative is therefore associated to the arithmetic mean of the square root of time. In the following the DL method was applied with this minor modification.

The DL method consists in adjusting Eq. (62) by linear regression fitting. However, the DL method is only a method to determine the values of the two parameters in Eq. (3) without bias. The second step which consists in determining S and K using the C_1 and C_2 values can be achieved by different methods described in Vandervaere et al. (2000b) depending on the number of disk radii and pressure head values applied (see ST, MR, MS1 and MS2 methods in this paper). Although not always recommended by these authors, as only one infiltration test with one radius and one pressure was available, it is only the Single Test (ST) method which will be combined with the DL method in the following, what will be written DL-ST method. The sorptivity $S = C_1$ is therefore provided by the intercept with the origin and the hydraulic conductivity can be deduced from the slope of the regression $2C_2$ as follows.

$$K = K_i + \frac{3}{2-\beta}\left[C_2 - \frac{\phi S^2}{R(\theta_i - \theta_0)} - K_i\right] \tag{68}$$

This method was used for the analysis of the mini-disk infiltrometers performed by Irstea.

4.5. Comparison of the L06 and DL-ST methods

Both DL-ST and L06 methods use the same basic equations for short to intermediate times. The difference is that the parameters optimization is performed in the (I,t) space for L06

whereas the ($\dfrac{dI}{d\sqrt{t}}$, $\sqrt{t}$) space is used for DL method. In addition, the DL method only uses short to medium times for the optimization, whereas the L06 method also exploits long times. Nevertheless, it is expected that the parameters values optimized using the L06 method lead to consistent ($\dfrac{dI}{d\sqrt{t}}$, $\sqrt{t}$) space. In particular, for long times, the points should verify:

$$\left(\frac{dI}{d\sqrt{t}}\right)_{\infty} = 2\left[AS^2 + K_0\right]\sqrt{t} \tag{69}$$

It means that the points for long times should be aligned on a straight line, with a slope different to the one at short time steps and this straight line goes through the origin.

This property will be used to compare the results of the L06 and DL-ST methods in the following.

5. Results

5.1. Distribution of the sample points, texture and particle size distribution

In order to analyze the sampled points, they can be classified according to various factors. The following were considered: land use, soil cartographic unit UC, geology, fraction of coarse fragments. The points' distribution according to those criteria is provided in Table 5-1, showing that the sampling is not homogeneous amongst classes.

Table 5-1: Number of sampled points according to various typologies for Beerkan and mini-disk infiltration tests. The total number of Beerkan points is 52 and of that of mini-disk points is 38.

	Land use						
	Cultivated grassland 10	**Permanent grassland 11**	**Catered grassland 12**	**Broad leaf forest 20**	**Coniferous forest 21**	**Landes and moors 22**	**Vineyard 30**
Beerkan	12	6	6	10	3	6	9
Mini-disk	12	5	4	5	3	4	5
	UC						
	8	**26**	**27**	**29**	**33**	**64**	**65**
Beerkan	9	5	7	10	9	6	6
Mini-disk	11	3	2	6	8	3	5
	Geology						
	Basalt			**Limestones**			
Beerkan	12			42			
Mini-disk	8			30			
	Fraction of fine soil						
	Class 1: >95%		**Class 2: 85-95%**		**Class 3: <85%**		
Beerkan	23		17		12		
Mini-disk	20		11		7		
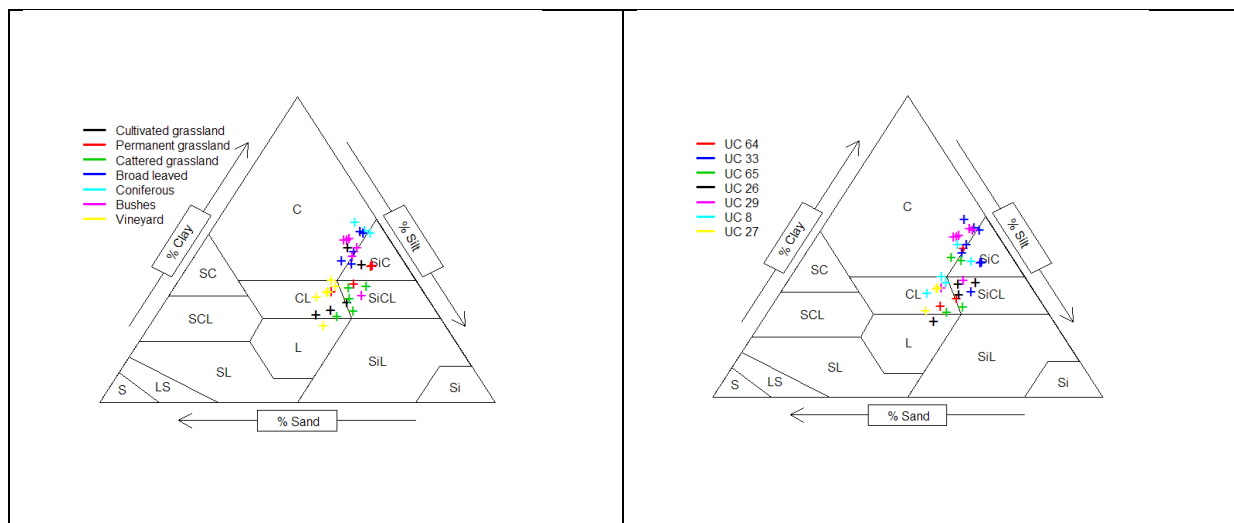
Figure 5-1: Location of the sampled points in the USDA textural triangle with different colors corresponding to land use (right) and soil typological unit (UC) (left)

The soil class of the sampled points is plotted in the USDA triangle in Figure 5-1 for the various land uses and soil mapping units (UC) of the BD-Sol Ardèche soil data base.

Figure 5-1 shows that soil texture in the Claduègne catchment is mostly composed of clay, clay loam, silty clay loam and silty clay, with one point located in the loam class. Figure 5-1a also shows that sample points located in broad leaf forests, coniferous forests and to a lesser extend bushes are located in the finer soils: clay and silty clay. It may be related to the fact that those soils are less favorable to agriculture.
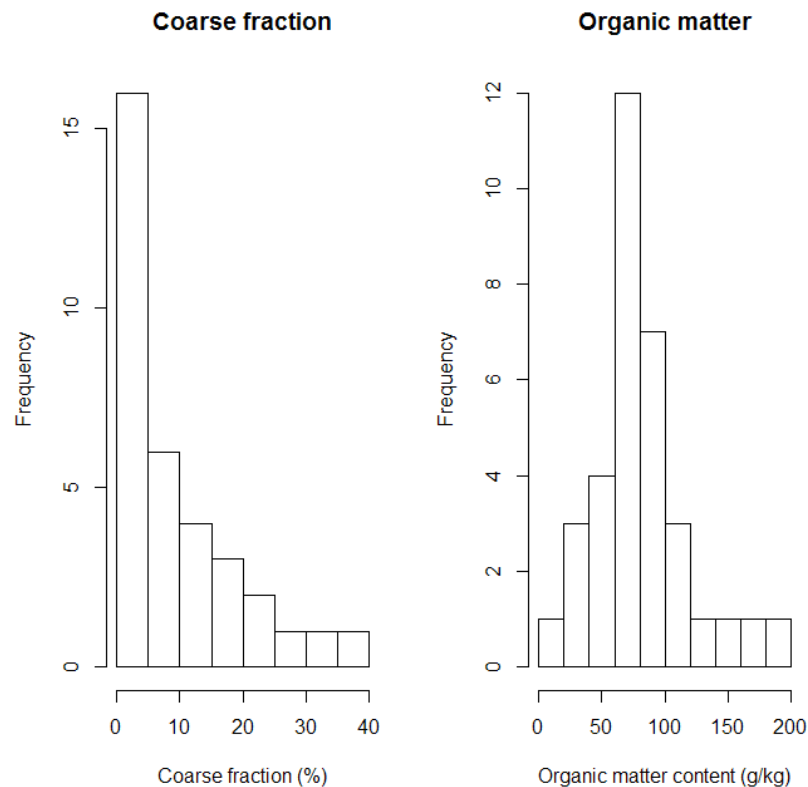
Figure 5-2: Histogram of coarse fraction and organic matter content

Table 5-2 provides the statistics of the particle size data, coarse fragments and organic matter contents of the sample points (34 points). The table also provides the shape parameters of the retention and hydraulic conductivity curves presented in section 4.3 (Eqs. (33) to (42)). Figure 5-2 provides histograms of coarse fraction (sum of gravels and stones) and of organic matter contents over the whole sample.

As already visible on the textural triangle, the sampled soils have a high fraction of clay and a low fraction of sand. We also note that more than 50% of the points have coarse fraction lower than 5%, but it can reach values as high as 40% (Figure 5-2-left). Organic content is high (Figure 5-2-right) in forests and bushes and the value is significantly larger than in cultivated points (value of the Kruskal-Wallis test is *p*=0.0033).

In terms of shape parameters of the retention curve, the *n* parameter has a very low range, with a CV of 1%. The shape parameter of the hydraulic conductivity curve η has a larger variability amongst soils with a CV of 18%. Note also that the median value of η is large (25.17) which is consistent with the high clay content. This also means that the hydraulic conductivity decreases very rapidly from saturation.

According to the Kolmogorov-Smirnov test, the hypothesis of normal distribution cannot be rejected at the 5% level, except for the d_g parameter.

Table 5-2 : Statistics of the particle size data

	Mean	Minimum	Maximum	Median	Standard deviation	CV
Organic carbon (g/kg)	46.13	8.81	112.00	44.45	22.36	0.48
Organic matter (g/kg)	79.81	15.20	194.00	76.85	38.72	0.49
Fine soils <2mm	0.91	0.63	1.00	0.95	0.11	0.12
Gravels 0.2-0.5 cm	0.02	0.00	0.09	0.01	0.03	1.28
Stones >0.5cm	0.07	0.00	0.31	0.04	0.09	1.27
Clay : <2μm	0.43	0.25	0.59	0.44	0.10	0.24
Fine silt : 2μm-20μm	0.28	0.24	0.34	0.27	0.03	0.11
Coarse silt : 20μm-50μm	0.13	0.08	0.20	0.13	0.03	0.26
Fine sand : 50μm-2000μm	0.07	0.02	0.15	0.07	0.04	0.49
Coarse sand : >2000μm	0.08	0.01	0.21	0.06	0.06	0.71
d_g (μm)	155.80	32.35	471.46	98.30	126.73	0.81
A	0.09	0.07	0.12	0.09	0.01	0.16
B	2.20	2.16	2.27	2.19	0.04	0.02
pA	0.19	0.15	0.24	0.18	0.03	0.16
pm	0.09	0.06	0.13	0.08	0.02	0.20
m	0.04	0.03	0.06	0.04	0.01	0.20
n	2.09	2.07	2.14	2.09	0.02	0.01
η	24.98	17.80	33.53	25.17	4.44	0.18
C_{p_VG}	2.65	2.51	2.77	2.66	0.08	0.03

5.2. Dry bulk density

Statistics of dry bulk density and final water content (assumed to be equal to saturated water content) are provided in Table 5-3. The median value of dry bulk density is 0.96 g cm^{-3} which is quite low with a coefficient of variation of 26%, showing the large variability of dry bulk density. The median value of saturated water content is 0.58, a large value consistent with the low median value of dry bulk density. The distribution of dry bulk density can be considered as normal at the 5% level according to the Kolmogorov-Smirnov test.

Figure 5-3 provides boxplots of dry bulk density (2.5 cm height cylinders) as function of various factors (land use, soil UC, geology, coarse fragments class – see definition in Table 5-1.

Statistical tests were performed to assess if the differences in variance, mean and distribution were significantly different amongst the different factors using the Fisher test, Student test and Wilcoxson rank sum test respectively. The analysis was performed using the *var.test*, *t.test* and *wilcox.test* functions of the R software. A Tukey Honest Significant Differences test (Tuckey HSD test) was also performed to confirm the results using the *TukeyHSD* function of the *stats* package in R (this approach can safely be used as the distribution of dry bulk density can be considered as normal). The detailed results are provided in Appendix 1 (Table A 1 to Table A 4). The results show that dry bulk density is significantly different between several UC classes and we can distinguish two main groups (Wilcoxon tests).

- Group 1: UC 29, 33, 64, 65
- Group 2: UC 8, 26, 27

As can be seen in Figure 5-3, samples points in group 1 have a much lower dry bulk density than those in group 2. In terms of land use, we can also distinguish two main groups, with group 1 having a much higher dry bulk density than group 2. We note that land uses in group 1 are mainly cultivated lands.

- Group 1: land use 10 and 30

- Group 2: land uses 11, 12, 2, 21, 22
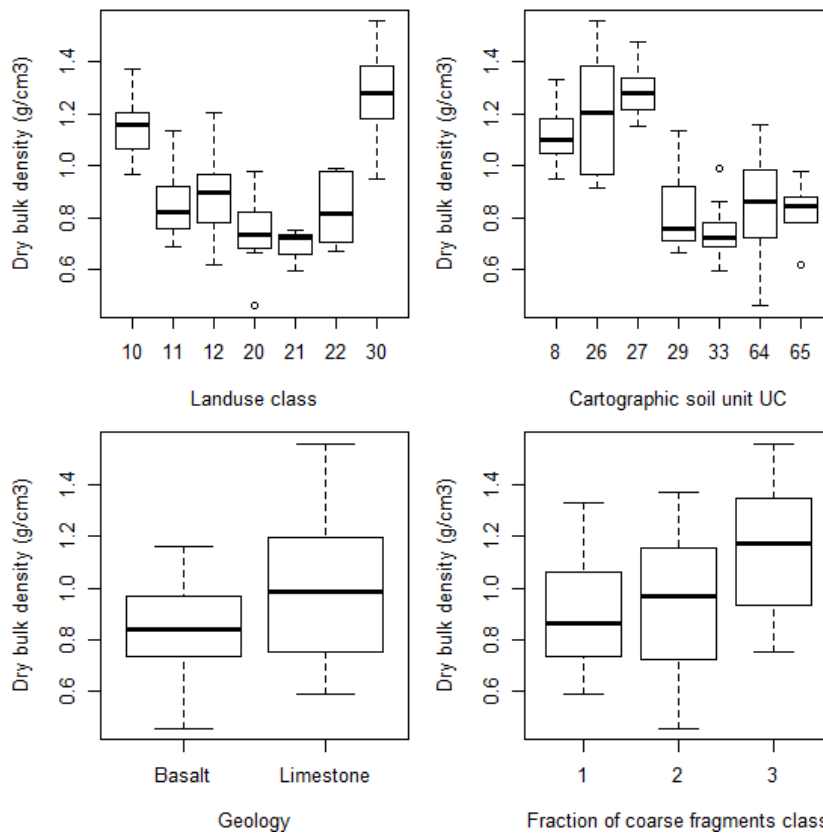
Figure 5-3: Boxplot of dry bulk density (2.5 cm height cylinder) according to land use, UC soil class, geology and fraction of coarse fragments (see definition of classes in Table 5-1
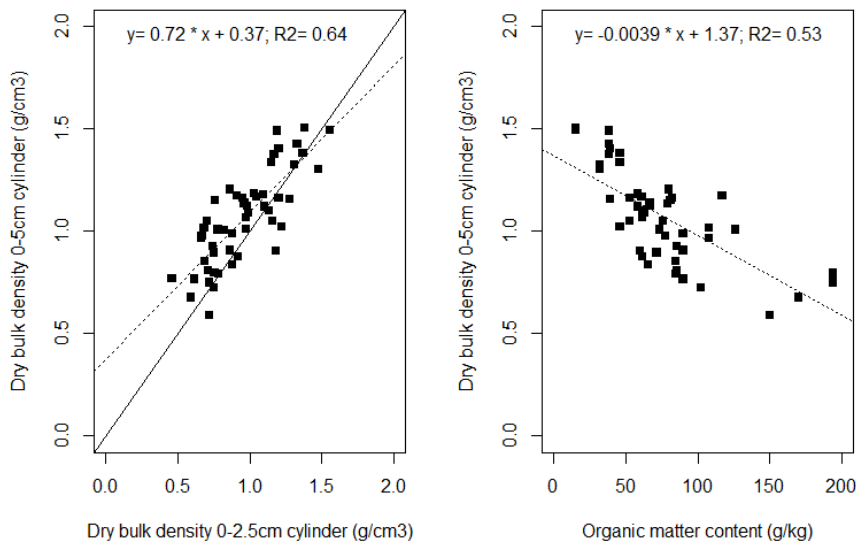
Figure 5-4: (Left) Comparison of dry bulk density measured using a small (2.5 cm height) and a large cylinder (5 cm height). (Right) Relationship between dry bulk density obtained with the 2.5 cm height cylinder and organic matter content

Dry bulk density was measured using small (2.5 cm height) and large cylinders (5 cm height) (Figure
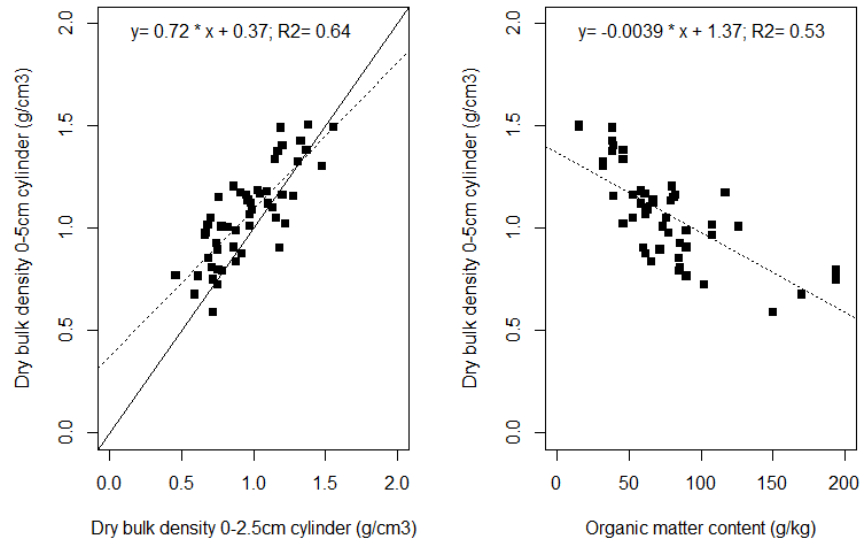
5-4a). Figure 5-4

b shows the correlation between dry bulk density obtained with the 2.5 cm height cylinders and organic matter content. The relationship is good with R^2=0.53 and, as expected dry bulk density decreases with increasing organic matter content.
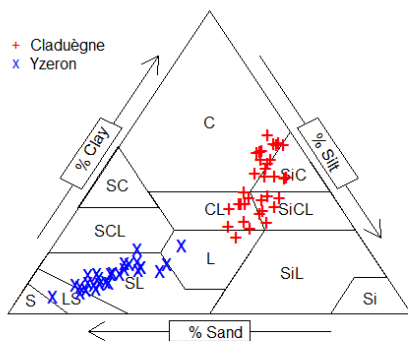
Figure 5-5 : Textural triangle where the data from the Claduègne infiltration tests are shown in red, and those from the Yzeron infiltration tests are shown in blue.
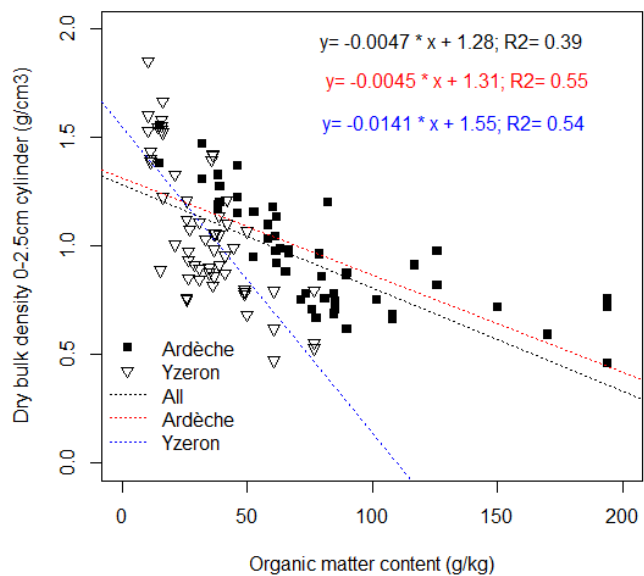
Figure 5-6: Correlation between dry bulk density obtained with the 2.5 cm height cylinders and organic matter for the data sets from Claduègne and Yzeron catchments

In order to see if this type of relationship can be generalized, data from the Claduègne campaign and those collected in the Yzeron catchment (south west of Lyon) by Gonzalez-

Sosa et al. (2010) are pooled together. Figure 5-5 shows the two data sets in the USDA textural triangle. It shows that soils from the Yzeron catchment are coarser than those of the Claduègne catchment (mostly loamy sand and sandy loam). Figure 5-6 shows than the same kinds of relationships between top soil dry bulk density and organic matter are obtained in both catchments with similar values of R^2, but a quicker decrease of dry bulk density with increase in organic matter content in the Yzeron catchment than in the Claduègne one. When the two data sets are mixed, the correlation is still significant but much lower (R^2=0.39). Organic matter content appears as a good predictor of dry bulk density of top soils.

5.3. Results using the L06 method for Beerkan and mini-disks infiltration tests

5.3.1. Presentation and discussion of data processing

The analysis of the infiltration tests was performed using the L06 method using values of β=0.6 and ϕ=0.75. It was assumed that the measured final water content was equal to the saturated water content. The optimization of Eq. (53) was performed using a function developed in the R package (R Development Core Team, 2015) and the *nlm* function of the *base* package.

Visual inspection of the infiltration time series was used to select the points retained in the optimization. Points could be removed at the beginning of the series due to quick infiltration and inaccuracy due to the movement of the water surface in the cylinder when removing the plastic. At the end of the infiltration test, points were also sometimes removed due to visible change in the slope of the curve, due to possible sampling of different soil horizons (sometimes increase of the infiltration velocity was even observed).

Examples of the types of results obtained for the *Beerkan* method are provided in Figure 5-7.

We also provide the T_{stab} value which is defined by Vandervaere et al. (2000b) as the time when vertical capillary forces become dominated by the two other terms of the equation (gravity and lateral diffusion):

$$T_{stab} = \left[\frac{S}{\frac{2-\beta}{3}(K_0 - K_i) + \frac{\phi S^2}{R(\theta_0 - \theta_i)}} \right]^2 \tag{70}$$

The different values of T_{stab} illustrate the accuracy of the method. For *Beerkan* 14.1, T_{stab}=40 s and the infiltration test lasts about 100 s. Therefore both S and Ks can be estimated accurately as the two regimes (short and long time are well sampled). For *Beerkan* 82b.4, T_{stab}=40 s and the infiltration test lasts about 2500 s. S is well estimated and K_s not so well as the long term regime is not very long. For *Beerkan* 82b.3, T_{stab}=300 s and the infiltration test lasts about 3000 s. In this case, there are only one-two points for describing short term regime and a lot of points for the long term regime. Therefore S is not well estimated whereas K_s can be estimated accurately. Finally, for *Beerkan* 74c.1, T_{stab}=2700 s and the infiltration test lasts only 900 s. Therefore S can be well estimated whereas K_s cannot, as the permanent regime is not reached due to the length of the infiltration test.
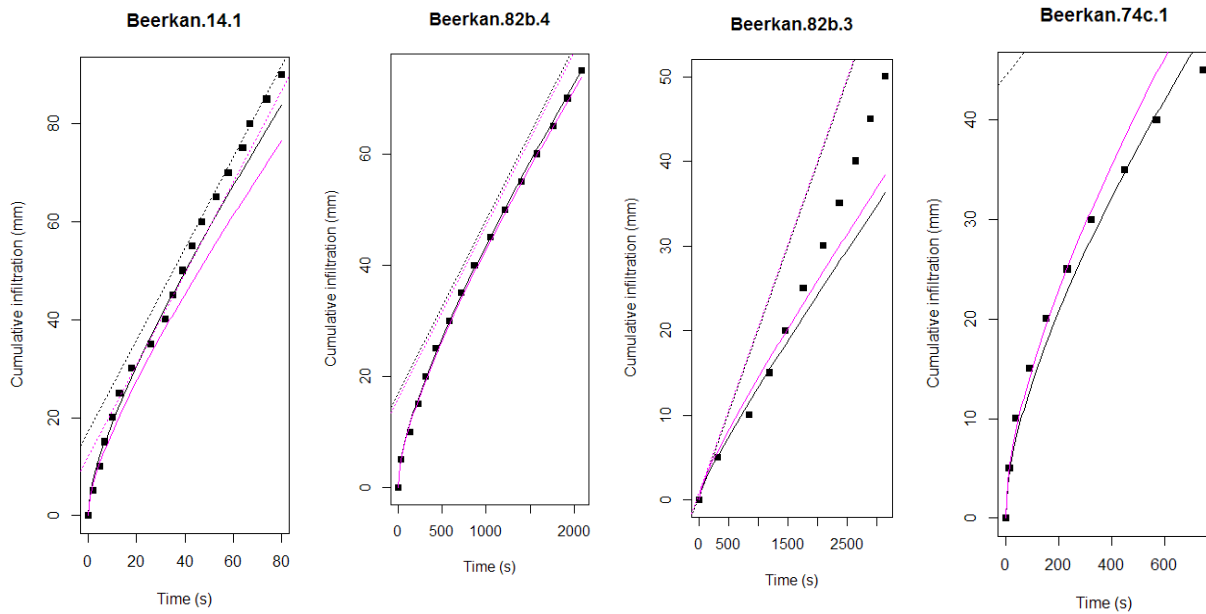
Figure 5-7: Examples of infiltration tests and of the fitted model using Eq. (50) for cumulative infiltration I (black) and infiltration flux q (pink). The dotted straight lines correspond to the equation for long times. (a) Point 14.1 with T_{stab}=40s. (a) Point 82b.4 with T_{stab}=1300s. (a) Point 82b.3 with T_{stab}=300s. (a) Point 74c.1 with T_{stab}=2700s.

A visual inspection was conducted and the various infiltration tests were assigned a quality index: 1 (good); 2 (quite good); 3 (fair); 4 (bad); 5 (rejected). This index was used for sample points selection in the statistical analysis presented in section 5.6.

For the mini-disk infiltration tests, points were also removed at the beginning of the series to remove the effect of the sand layer as recommended by Vandervaere et al. (2000a). The cumulative infiltration data and cumulative time were modified using a translation on both *I* and *t* axes, before any other calculation. For some infiltration tests performed using the mini-disk, an acceleration of the flow was sometimes observed at the end of the test, which is in contradiction with the used theory. In this case, points at the end of the test were also removed. Figure 5-8 provides an example of such a case.
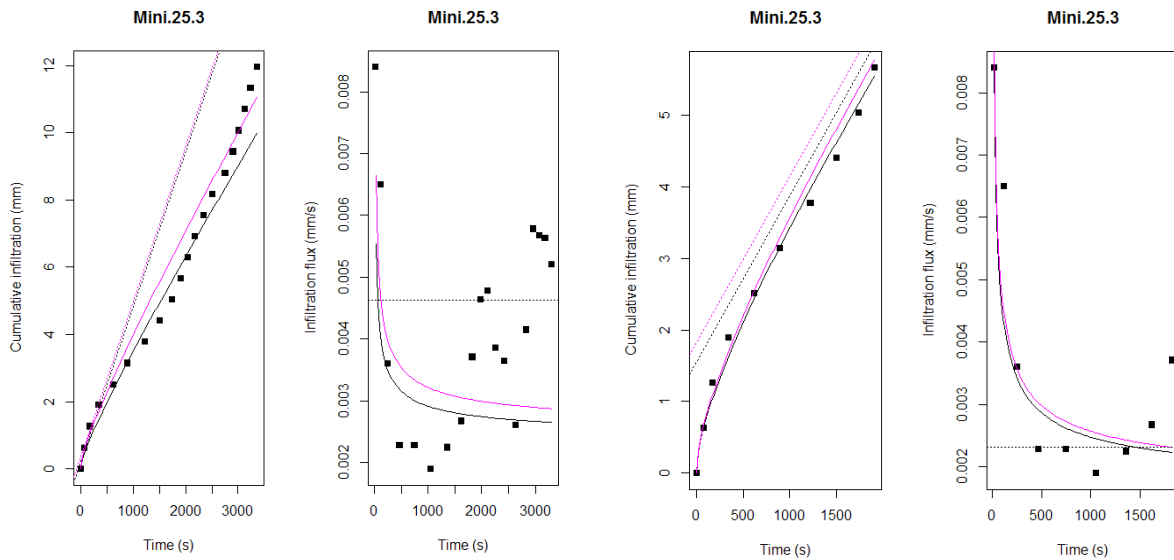
Figure 5-8: Example of a mini-disk infiltration test where acceleration of the flow was observed (left). Same infiltration test, after points selection (right). In this case a value of $K_s=15$ mm h-^{1} is obtained. The figure provides both the fit on cumulative infiltration (black) and infiltration flux (pink).

In section 4.3, we introduced two possible methods for estimation of the parameters using the L06 method, called Method 1 (where the slope of the long term regime straight line is used to assess K_0) and Method 2 (where the intercept of the long term regime straight line is used to assess K_0). Figure 5-9 shows an example of such comparison for the *Beerkan* infiltration tests optimized using the infiltration flux data but the results are similar for mini-disks and optimization on the infiltration flux. It shows that the agreement is very good on sorptivity with R^2 close to 1.On the other hand, K_s and λ_m values obtained using Method 1 are systematically lower than with Method 2. A systematic difference is also observed on the *hg* parameter.
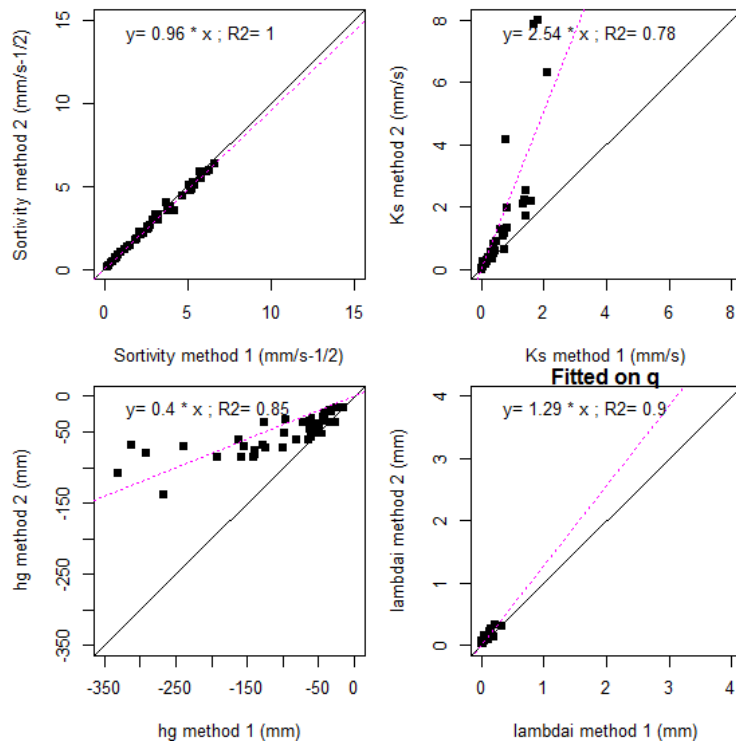
Figure 5-9: Comparison of the results between Method 1 and Method 2 for the Beerkan infitltration tests for sorptivity, hydraulic conductivity, h_g parameter and pore size radius λ_m. Parameters are fitted using the cumulative infiltration q.
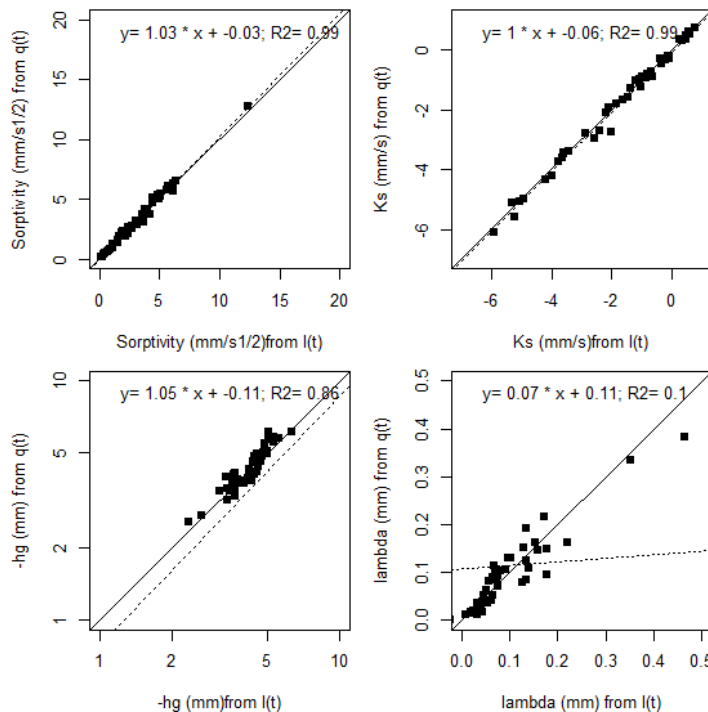
Figure 5-10: Comparison of Method 1 results obtained when the optimization is performed on cumulative infiltration or on the infiltration flux for sorptivity, saturated hydraulic conductivity, h_g parameter and pore size radius for the Beerkan infiltration tests.

The computation was also performed using optimization on cumulative infiltration *I* or infiltration flux *q*. The results are compared in Figure 5-10 and Figure 5-11 for *Beerkan* and

mini-disk infiltration tests respectively. The figures show that results in terms of sorptivity, hydraulic conductivity and h_g (for the *Beerkan* tests) are very similar with values of R^2 larger than 0.93. Differences are more noticeable when comparing the estimated pore radius with a larger dispersion. Given the large noise on the infiltration flux, those results are considered as very satisfactory.
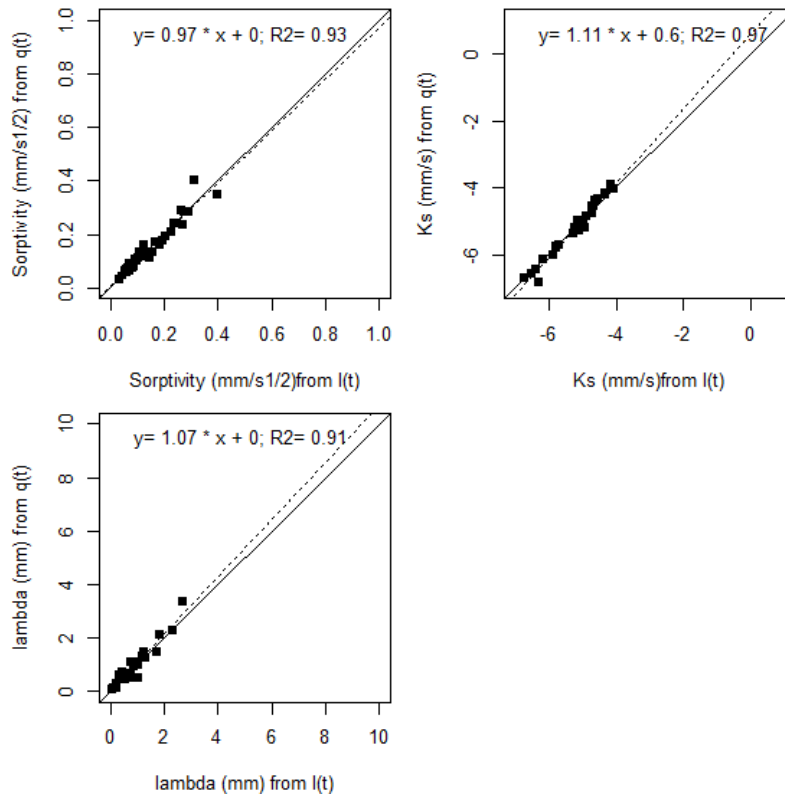
Figure 5-11: Comparison of Method 1 results obtained when the optimization is performed on cumulative infiltration or on the infiltration flux for sorptivity, saturated hydraulic conductivity and pore size radius for the mini-disk infiltration tests.

The mini-disk infiltration tests were performed either with the small (∅ 4.5 cm) and large (∅ 8 cm) diameters. The results were generally found to be more stable with the larger diameter, which is expected as the contact surface between the apparatus and the soil is larger. Comparison between the results obtained with both diameters is only possible at a small number of points. This comparison is provided in Figure 5-12. It shows a quite large dispersion of the results between the two diameters; especially for K_s (the graph is provided in log scale). The dispersion in terms of pore size diameter is also large. We can also note the high values of this pore size diameter (about 1-2 mm) which would mean that pore of this size are activated.
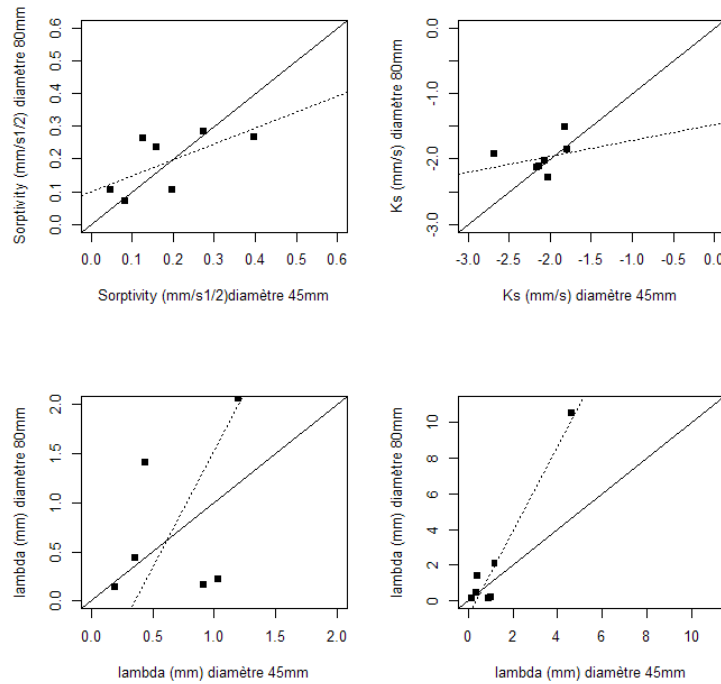
Figure 5-12: Comparison of the mini-disk results between using the small (4.5 cm) and large (8 cm) diameter infiltrometers. The bottom left figure is a zoom of the bottom right one showing an outlier on the pore size radius.

5.3.2. Statistical description of the results

Statistics of the calculated sorptivity, hydraulic conductivity and *hg* parameter (only for *Beerkan*) are provided in Table 5-3 for calculations performed using either the cumulative infiltration or the infiltration flux.

For the *Beerkan* infiltration tests, we also provide the maximum infiltration time t_{max} which correspond to the time needed to infiltration the 12 l water volume (corresponding to a 95.5 mm water height). We also computed the infiltration capacity $L_{max} = 95.5/t_{max}$. We can see that infiltration was sometimes terminated in a few seconds, whereas some other tests lasted several hours. The median value is 163 s, ie. less than 3 minutes. The median infiltration capacity is also very large (0.58 mm s^{-1}, i.e more than 2000 mm h^{-1}). The variability of t_{max} and L_{max} is also very large with CV of 1.83 and 1.52 respectively.

For the *Beerkan* infiltration tests, the median of saturated hydraulic conductivity is very high (about 0.35 mm s^{-1}, more than 1200 mm h^{-1}), with a coefficient of variation of 1.9. The distribution is not normal (Kolmogorov Smirnov test with *p*=0.0002). However, a log normal distribution is acceptable (Kolmogorov Smirnov test with *p*=0.36). The variability of sorptivity is also high (0.78).

The hydraulic conductivity at -20 mm, deduced from the mini-disk, is much lower than the value of K_s, as the median value is 0.0061 mm s^{-1} (22 mm h^{-1}) for the optimization on *I* and for the optimization on *q*. The coefficients of variation are nevertheless much higher than for K_s (3.7 for the optimization on *I* and 5.6 for the optimization on *q*). The robustness of the estimation is therefore lower for the mini-disk than for the *Beerkan*, probably due to the difference in sampling surface.

Table 5-3: Statistics of dry bulk density (2.5 cm height cylinder), final water content and computed sorptivity, hydraulic conductivity and hg parameter for the Beerkan method and sorptivity, hydraulic conductivity for h=-20mm for mini-disk infiltrometers. Values indexed by _I were computed using cumulative infiltration and values indexed by _q using the infiltration flux.

	Mean	Minimum	Maximum	Median	Standard deviation	CV	Number of points
					Beerkan		
Dry bulk density (g cm^{-3})	0.96	0.46	1.55	0.96	0.25	0.26	52
Final water content (m^3 m^{-3})	0.57	0.37	0.74	0.58	0.08	0.15	52
t_{max} (s)	840	9	6977	163	1543	1.83	52
L_{max} (mm s^{-1})	1.37	0.043	10.61	0.58	2.08	1.52	52
S_I(mm $^{s-1/2}$)	3.35	0.13	13.45	3.09	2.62	0.78	50
K_{s_I}(mm s^{-1})	0.80	0.003	8.35	0.34	1.52	1.89	50
h_{g_I}(mm)	-97.16	-575.66	-10.66	-75.50	88.71	0.91	50
S_q(mm $^{s-1/2}$)	3.21	0.16	12.77	2.92	2.27	0.71	49
K_{s_q}(mm s^{-1})	0.62	0.002	6.67	0.35	1.05	1.68	49
h_{g_q} (mm)	-120.20	-456.33	-12.97	-63.20	110.88	0.92	49
					Mini-disk		
S_I(mm $^{s-1/2}$)	0.141	0.011	0.397	0.116	0.090	0.640	37
K_I(mm s^{-1})	0.017	0.0004	0.382	0.006	0.061	3.671	37
S_q(mm $^{s-1/2}$)	0.145	0.145	0.145	0.145	0.091	0.629	33
K_q (mm s^{-1})	0.007	0.0001	0.020	0.006	0.043	5.810	33
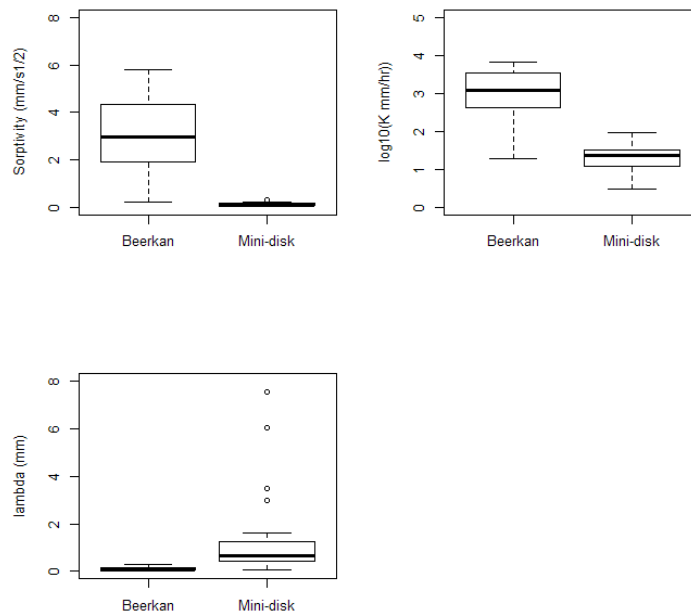
Figure 5-13: Boxplot of the parameters obtained using the Beerkan and mini-disk for sorptivity, hydraulic conductivity and active pore size radius. The boxplot are drawn with 22 sample points where both an estimate of the Beerkan and mini-disk infiltrometers was available.

Boxplot of the different parameters obtained with the *Beerkan* and mini-disk are provided in Figure 5-13 which confirms the difference in median for the hydraulic conductivity between the two methods. Note that the boxplot are provided in log scale for the hydraulic conductivity. The ratio between the median value at saturation and close to saturation (*h*=-20

mm) is about 57 which shows that the role of macropores and preferential flow is large at saturation.

We also performed Fischer, Student and Wilcoxon statistical tests to identify if differences in variance, mean and distribution could be identified between soil classes and land use classes for the logarithm of saturated hydraulic conductivity obtained using the *Beerkan* infiltration tests. The details are provided in Table A 6 for the analysis according to soil classes and Table A 7 for the analysis according to land use classes. We provide the boxplot in Figure 5-14.
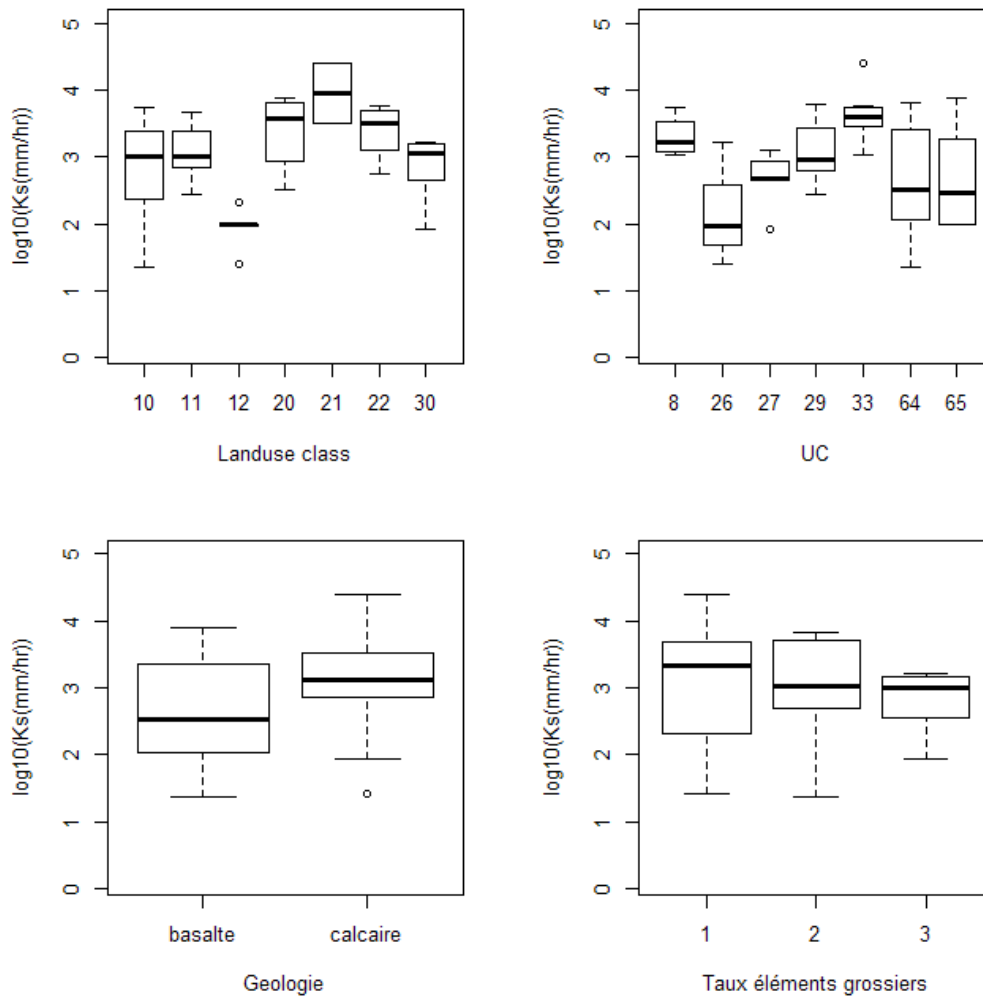
Figure 5-14: Boxplot of logarithm of saturated hydraulic conductivity derived from the Beerkan infiltration tests according to land use, UC soil class, geology and fraction of coarse fragments (see definition of classes in Table 5-1)

Those results highlight that soil class UC 33 can be distinguished from the others. But no significant differences can be evidenced for the other soil classes.

In terms of land use, it is possible to distinguish three groups with significantly different distributions.
- Group 1: land use 12 (catered pasture)
- Group 2: land use 10, 11, 30 (cultivated and natural grassland, vineyard)
- Group 3: land use 20, 21, 22 (broad leaf and coniferous forest, moors and fallow

This result suggests a significant impact of land use on the soil saturated hydraulic conductivity which is examined more in depth in section 5.6.

For the mini-disk results, no significant difference was found when soil classes or land uses were considered as factors (not shown).

5.4. Comparison between the L06 and DL-ST method for the mini-disks

For the mini-disks, the data were also analyzed using the DL-ST method, presented in section 4.3 and 4.4. As the DL-ST method is only applicable for short to medium time steps, results obtained with the L06 method were used for selecting the points used in the DL method fitting. In addition, we systematically plotted on the same graph the L06 analysis results translated in the ($\frac{dI}{d\sqrt{t}}$, $\sqrt{t}$) space and the straight line which can be adjusted for long time in this space (see Eq. (69)). In this application we used values of β=0.6 and ϕ=0.75.

A first point which is illustrated in Figure 5-15 concerns the point selection and the impact of the sand layer. In the analysis, when points at the beginning of the infiltration tests were considered impacted by the sans layer, a translation of the data cumulative infiltration and time was performed, so that the first points correspond to (0,0). This manipulation has consequences on the DL fit as the values of ($\frac{dI}{d\sqrt{t}}$, $\sqrt{t}$) are different than if the translation had not been performed.
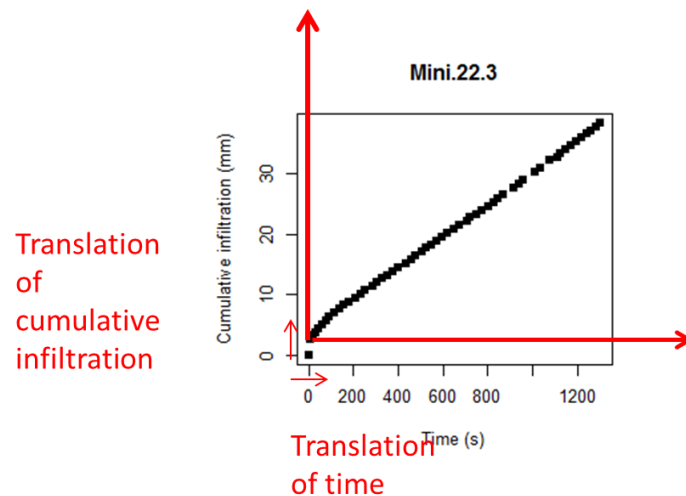
Figure 5-15: Illustration of the data processing when points are removed at the beginning of the infiltration test.

This impact is illustrated in Figure 5-16 and Figure 5-17 for one mini-disk infiltration test. By comparing the DL method results in Figure 5-16 and Figure 5-17, we can see that the removal or not of points at the beginning of the infiltration test has a large impact on the estimated regression, with a larger value of C_1 when the translation is not performed and lower value of C_2.

We also note in the figures that Eq.(69) is relevant and that the points for longer times can be adjusted using a straight line going through the origin. We also note the change of slope between the two parts of the curve. This rupture in the slope could be used to determine which points belong to the first part and which points belong to the second one. But it is not always

easy to see this rupture. The use of the L06 method for the determination of the number of points belonging to the first part is a less subjective alternative. Note also that, in the present application of the DL-ST method, we have not used the second part of the curve, although it conveys some information.
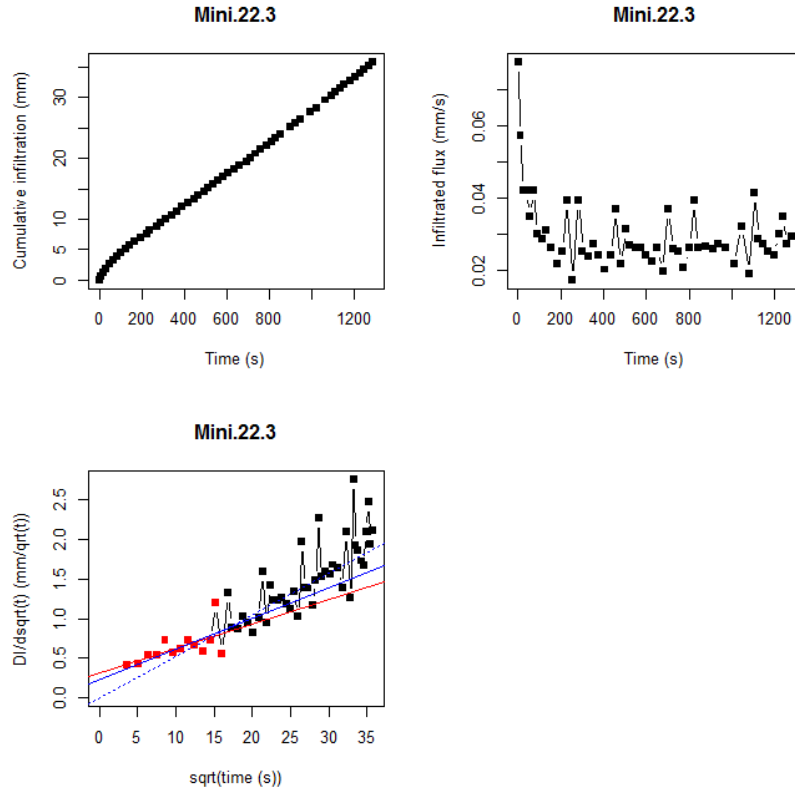
Figure 5-16: Analysis of mini-disk infiltration test using the DL-ST method. We first plot the cumulative infiltration as function of time (top left), the infiltration flux (top right) and the data in the (

$$\frac{dI}{d\sqrt{t}} , \sqrt{t})$$ *space. Points in red are those selected for the DL regression line fit and the red line is the*

corresponding regression line. The full blue line is the regression line obtained when computing C_1 and C_2 from the L06 results and the blue dotted line is the long term straight line provided by Eq. (69. Note that in this figure the points removed at the beginning of the infiltration test do not appear and the cumulative infiltration and infiltration time were modified (translation) before data analysis.

With the DL-ST method, we get C1=0.316 and C2=0.0154, leading to a negative value of K. With the L06 method, the L06 method provides a lower value of C_1=0.227 and a larger value of C_2= 0.0194 than the DL-ST method. Note however that the DL method provides the standard error of the parameters which leads to C_1=0.316 ± 0.129 and C_2=0.0058± 0.0058. The standard error of the estimated coefficient is large, due to the large points' dispersion, as compared to larger diameter infiltrometers.

On this example, the L06 values are within the ± one standard deviation range of the DL-ST estimated values, but the DL method leads to negative values of hydraulic conductivity, whereas the L06 method leads to a positive one. This point could be related to the choice of the values of β=0.6 and ϕ=0.75, which may not be relevant for all soils (e.g. Lassabatère et al., 2009; Nasta et al., 2012).

Differences between the estimates of the two methods may also be explained by the way the fitting is performed: in the $(\frac{dI}{d\sqrt{t}}, \sqrt{t})$ space, all the points have the same weight in the regression. On the other hand, as the fit is performed on cumulative infiltration using the RMSE criteria, higher weight is assigned to large values in the L06 optimization. With the L06 method, values of estimated hydraulic conductivity is generally positive, this is not the case for the DL-ST method.
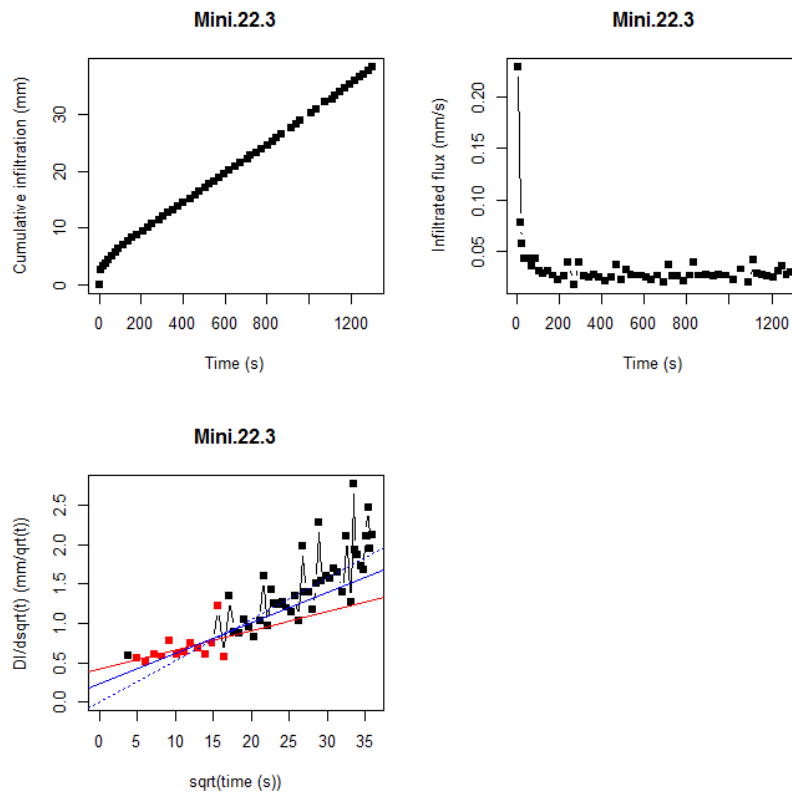
Figure 5-17: Same as Figure 5-16 but we have plotted all the points, including the first point which was removed (impact of sand layer). Even if the first point is not used in the regression (red points), the results are different than in Figure 5-16 because the value of I and t are different (no translation performed). With the DL-ST method, we get $C_1=0.415$ and $C_2=0.0121$, leading to a negative value of K.

The comparison of the results of the DL-ST and L06 methods on the whole sample is presented in Figure 5-18 and

Table 5-4 provides the statistics of the parameters for the two methods. The agreement between the two methods is satisfactory for the sorptivity with a R^2=0.87 but values are about 30% larger using the DL-ST method than with the L06 method. In terms of C_2, the agreement is also satisfactory with a R^2=0.77. Values are generally larger with the L06 method than with the DL method. The agreement on K remains fair with R^2=0.67, but values are about 64% larger with the DL-ST method than with the L06 method. Note also that about half of the infiltration tests provide negative values of K with the DL-ST method which seems to be more sensitive to inaccuracy in the measured data than the L06 method.

Table 5-4 : Statistics of the results of the L06 and DL-ST methods on the mini-disk infiltration tests. Negative values were discarded from the analysis.

	Mean	Minimum	Maximum	Median	Standard deviation	CV	Nbre points
$C_1 = S$ L06 method	0.148	0.035	0.400	0.126	0.091	0.61	34
$C_1 = S$ DL method	0.178	0.005	0.734	0.135	0.165	0.93	34
$C2$ L06 method	0.0111	0.0009	0.0482	0.0085	0.0097	0.87	34
$C2$ DL method	0.0099	0.0011	0.0282	0.0094	0.0064	0.64	34
K L06 method	0.0063	0.0010	0.017	0.0063	0.0045	0.71	21
K DL method	0.0147	$6.03 \ 10^{-5}$	0.0383	0.0082	0.0104	0.71	21
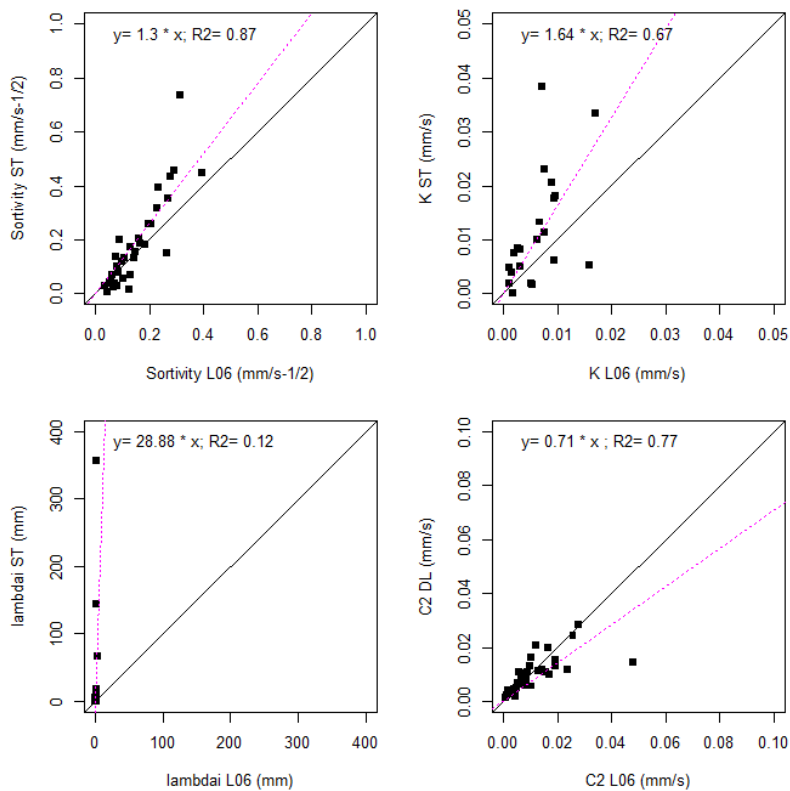
Figure 5-18: Comparison of the DL-ST and L06 method for the mini-disk infiltration tests. We show the comparison of $S=C_1$ (top left), K (top right), λ (bottom left) and C_2 (bottom right)

In Figure 5-19, we present the comparison of the sorptivity and C_2 coefficients obtained with the DL-ST method with their standard deviation for each infiltration test and the value of the L06 method is plotted on the same graphs. We can see, as expected that the sorptivity obtained with the L06 method are generally lower than the DL values, although most of them are located within the ± one standard deviation interval. When this is not the case, the C_2 coefficient obtained using the L06 method are also generally outside the ± one standard deviation interval of the DL-ST values.

From the comparison presented in this section, it is difficult to say that one method is performing better than the other. It is satisfying to see that both method give consistent results and that they generally agree on the order of magnitude of the parameters (see the quite good correlation in Figure 5-18). The L06 method seems to be more robust for the experimental conditions in which the infiltration tests were performed: small diameter and sometimes difficulties with the stability of the apparatus (due to windy conditions).

In the following, we will consider that the results obtained using the L06 method can be used with confidence for a comparison with standard pedo-transfer functions and the assessment of the impact on land use on the soil hydraulic properties. It allows performing the assessment with a larger sample size.
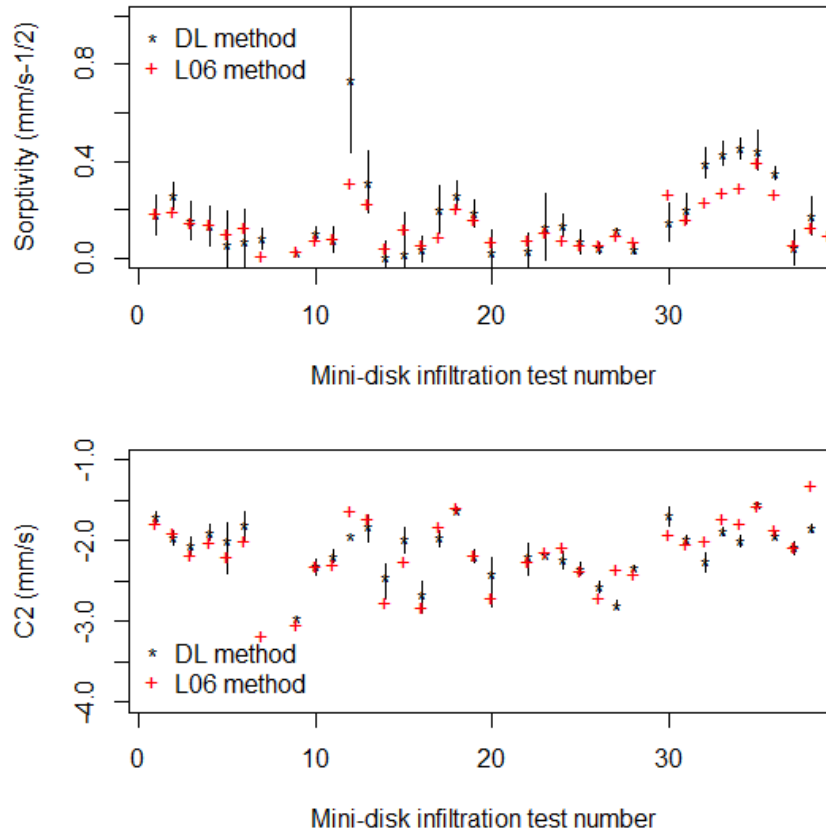
Figure 5-19: Comparison of sorptivity (top) and C₂ coefficient (bottom) obtained using the DL method (black stars ± one standard deviation) and the L06 method (red crosses) for the mini-disk infiltration tests.

5.5. Results of the LTHE infiltration tests using an infiltrometer and multiple suctions

In this section, we present the results obtained using the infiltration tests performed by LTHE using an infiltrometer with multiple suctions. The infiltrometer diameter was 10 cm. The data were analyzed using the method described in section 4.2. We provide the *K* values obtained at the various suctions and the extrapolated value of the saturated hydraulic conductivity in Table 5-5. The table also provides the values estimated using the L06 method for the same points.

When comparing the results obtained with the infiltrometer with multiple suctions and those derived from the L06 method, the following remarks can be done:

- The values obtained at *h=0* using the *Beerkan* method are generally much larger than the extrapolation of the infiltrometer with multiple suctions data. The ratio can range up to a factor 10. This is consistent with the fact that the *Beerkan* infiltration tests are performed using a positive head.

- On the other hand, the values obtained for h=-20mm with the mini-disk and L06 method are generally lower than the value obtained with the infiltrometer with multiple suctions.
- For saturated hydraulic conductivity, apart from point 14-2, the different points are ranked in a similar manner so both methods provide the same relative information about saturated hydraulic conductivity.

However, it is difficult to conclude on those differences as the difference may also be related to the local spatial variability of soil hydraulic properties which is known to be large.

Table 5-5: Values of the estimated hydraulic conductivity for the various pressures using the LTHE infiltrometer. We also provide in blue the values obtained at the same points using the Beerkan method (h=0) and the mini-disk (h=-20mm)

Point 14-2 (permanent pasture)						
h (mm)	-50	-30	-20	-7	0	
K (mm s^{-1})	0.00094	0.0055	0.0168 0.0094	0.0597	0.114 0.302	
Point 16-1 (coniferous forest)						
h (mm)	-27.5	-20	-12.5	-7.5	-5.0	0
K (mm s^{-1})	0.00362	- 0.000262	0.0213	0.0334	0.0423	0.0771 0.899
Point 25-1 (oak wood)						
h (mm)	-70	-55	-30	-15	-7.5	-5	0
K (mm s^{-1})	0.000645	0.000912	0.00386	0.0146 0.0483(h=-20mm)	0.0361	0.0525	0.0503 0.529
Point 74A-1 (cultivated grassland)						
h (mm)	-30	-20	-15	-7.5	-5	0
K (mm s^{-1})	0.0133	- 0.00423	0.168	0.564	0.525	1.475 1.500
Point 74B-2 (vineyard)						
h (mm)	-70	-55	-35	-20	-7.5	-5	0
K (mm s^{-1})	0.000645	0.000912	0.00436	0.0130 0.00729	0.0263	0.0313	0.0420 0.432

5.6. Statistical analysis of the data: impact of land use versus soil texture

In this section, we examine the relationship between the estimated hydraulic conductivity derived from in situ infiltration tests and the values deduced from pedo-transfer functions. We also explore the possible impact of land use on the soil hydraulic properties.

5.6.1. Comparison with classical pedo-transfer functions

Following the work performed by Manus (2007) and by Gonzalez-Sosa and Braud (2009), we computed the parameters from several pedotransfer functions representative of the various approaches existing in the literature. We chose the following pedotransfer function:

- the one proposed by Cosby et al. (1984) (C84 in the following), which only depends on soil texture (% clay, sand and silt)
- the one from Rawls and Brackensieck (1985) (RB85 in the following) which takes into account % clay, % sand and the porosity

- the one from Weynants et al. (2009) (W09 in the following) which is an update of the pedotransfer functions proposed by Vereecken et al. (1990) which takes into account the % clay, % sand, dry bulk density and organic carbon content.

The formulae of the various pedotransfer functions are provided in Appendix 3.

In the following, we only examine the comparison of the saturated hydraulic conductivity parameter between the various pedotransfer functions and the in situ values.

We could also have compared the values of saturated water content, n and h_g parameter of the Van Genuchten (1980) retention curve. However, this requires some data manipulation as the various pedotransfer functions do not directly provide the parameters for the Van Genuchten – Burdine retention model. So manipulations are required to transform the parameters of the Brooks and Corey (1984) model to the Van Genuchten one, or parameters for the Van Genuchten – Mualem to the Van Genuchten – Burdine model. For this purpose, the formulae proposed by Leij et al. (2005) can be used.
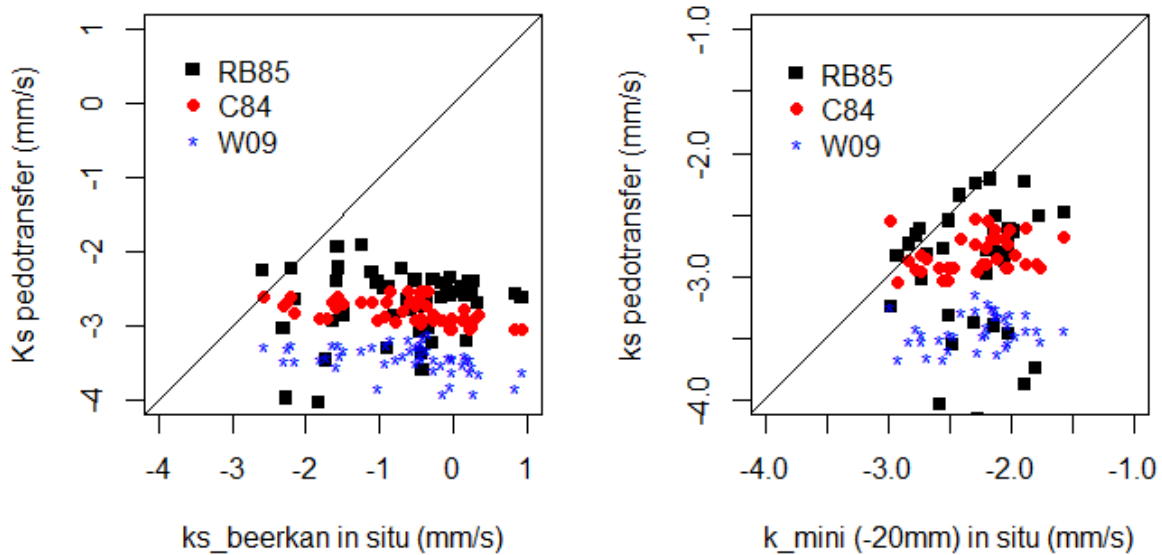
Figure 5-20: Comparison of the in situ saturated hydraulic conductivity derived from the Beerkan method (left) and the near saturation hydraulic conductivity K(-20mm) from the mini-disk (right) with the pedotransfer functions of Rawls and Brackensieck (1985) (RB85), Cosby et al. (1984) (C84) and Weynants et al. (2009) (W09)

The comparison of the various estimates is provided in Figure 5-20 and Table 5-6 provides the statistics of those estimates. The dispersion of C94 and W09 is much lower than that of RB85 and much less than the in situ values. In situ values are generally much larger than those of the pedotransfer functions (several orders of magnitude). The agreement is larger when the comparison is performed using the mini-disk in situ values, but this is expected as pedotransfer functions do not take macropores into account.

Nevertheless, none of the pedotransfer function is able to predict correctly the variability of the observed value. The RB85 function is the one which better reproduces the observed variability. This result was also mentioned by Manus et al. (2009) who choose the RB85 pedotransfer function as representative for describing the variability of soils in the Cévennes Vivarais region.

Table 5-6: Values of statistics of the saturated hydraulic conductivity calculated using the various pedotransfer function and the Beerkan and mini-disk. Values are provided in mm s-1

	Mean	Minimum	Maximum	Median	Standard deviation	CV	Nbre points
K_s RB85	$1.80 \ 10^{-6}$	$2.69 \ 10^{-8}$	$6.14 \ 10^{-6}$	$1.79 \ 10^{-6}$	$2.45 \ 10^{-6}$	1.36	52
K_s C84	$1.59 \ 10^{-6}$	$8.67 \ 10^{-7}$	$2.96 \ 10^{-6}$	$1.40 \ 10^{-6}$	$6.21 \ 10^{-7}$	0.39	52
K_s W09	$3.80 \ 10^{-7}$	$1.33 \ 10^{-7}$	$7.35 \ 10^{-7}$	$3.51 \ 10^{-7}$	$1.56 \ 10^{-7}$	0.41	52
K_s Beerkan	0.805	0.00265	8.35	0.344	1.52	1.89	52
K_s mini-disk	0.00694	0.00105	0.027	0.0625	$5.36 \ 10^{-3}$	0.77	32

5.6.2. <u>Impact of land use on the estimated soil hydraulic properties</u>

We have shown in section 5.2 that land use had a significant impact on dry bulk density and in section 5.4, that it was also the case for saturated hydraulic conductivity.
We finally distinguished the following classes for dry bulk density:
- DB1: land uses 11, 12, 20, 21, 22
- DB2: land uses 10, 30

and for saturated hydraulic conductivity:
- KS1: land uses 20, 21, 22
- KS2: land uses 10, 11, 12, 30

Table 5-7: Statistics of the soil hydraulic parameters (dry bulk density, saturated hydraulic conductivity, hydraulic conductivity at -20 mm, scale parameter h_g of the retention curve, pore size diameters

	Mean	Minimum	Maximum	Median	Standard deviation	CV
DB1 dry bulk density (g cm^{-3})	0.804	0.461	1.200	0.757	0.157	0.19
DB1 dry bulk density (g cm^{-3})	1.197	0.905	1.555	1.180	0.164	0.14
KS1 K_s (mm s^{-1})	1.728	0.0928	8.345	0.925	2.24	1.30
KS2 K_s (mm s^{-1})	0.285	0.00265	1.500	0.166	0.369	1.29
KS1 h_g (mm)	-90.34	-211.2	-10.66	-67.79	64.41	0.71
KS2 h_g (mm)	-101.0	-575.7	-14.44	-75.50	100.6	1.00
KS1 λ (mm)	1.405	<0	12.54	0.065	3.92	2.79
KS2 λ (mm)	0.348	0.0092	4.98	0.070	1.05	3.01
KS1 $K_{(-20mm)}$ (mm s^{-1})	0.00334	0.00119	0.0076	0.0024	0.00225	0.67
KS2 $K_{(-20mm)}$ (mm s^{-1})	0.0083	0.00105	0.0271	0.00728	0.00556	0.67
KS1 λ (min-disk) (mm)	0.97	0.088	2.677	0.896	0.703	0.72
KS2 λ (minidisk) (mm)	0.656	0.0339	2.307	0.443	0.593	0.90
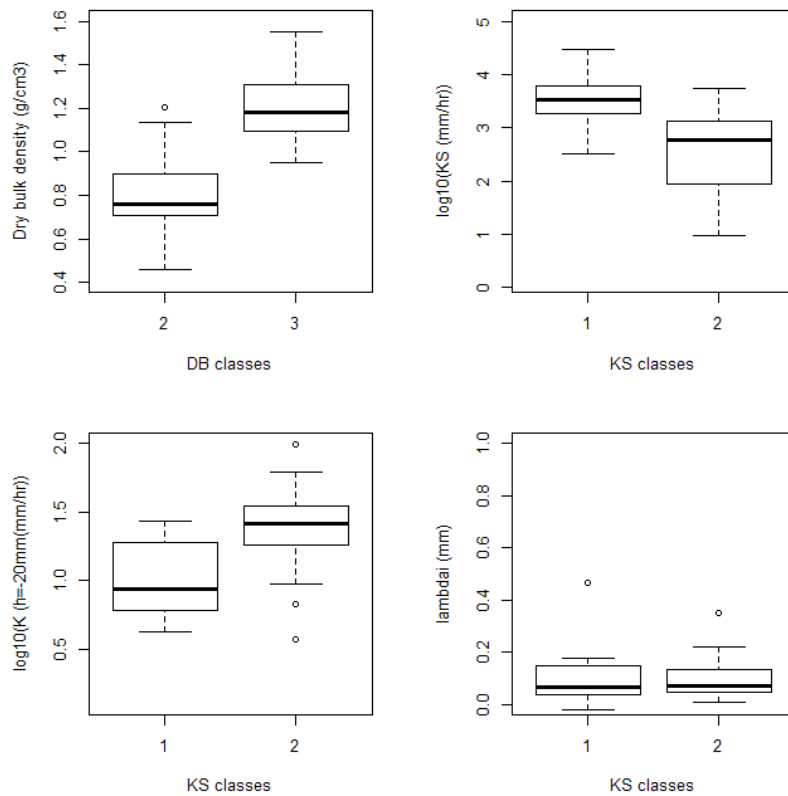
Figure 5-21: Boxplot of dry bulk density with regards to DB land uses classes (top left), logarithm of saturated hydraulic conductivity (top right), hydraulic conductivity at -20 mm (bottom left) and pore size distribution diameters (bottom right) for the KS land uses classes

We provide the values of the statistics of the parameters in the various classes in Table 5-7 and Figure 5-21 shows the corresponding boxplots.

The *p* values of the Kruskal-Wallis test is <0.001 for dry bulk density and saturated hydraulic conductivity which shows a significant difference at the 1% level. It is 0.003 for hydraulic conductivity at -20mm which shows a significant at the 5% level.

The results highlight that "natural soils" have a much lower dry bulk density than cultivated soils. Forested soils have also a much larger saturated hydraulic conductivity than cultivated soil, but the reverse is true for near saturated hydraulic conductivity at -20mm. We also note that the median value of pore size diameters is larger for the mini-disk than for the *Beerkan* infiltration test, which is not logic, but may be due to the lower robustness of mini-disk data analysis (due to the smaller device diameter as compared to the *Beerkan* method).
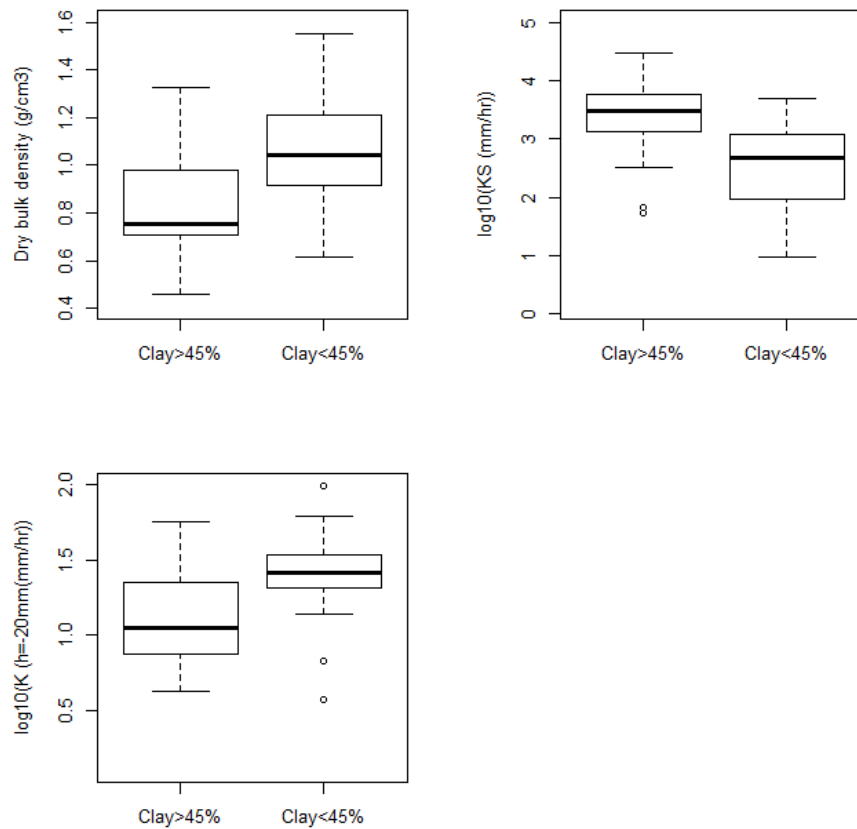
Figure 5-22: Boxplot of dry bulk density (top left), logarithm of saturated hydraulic conductivity (top right), hydraulic conductivity at -20 mm (bottom left) for two clay content classes (lower or higher than 45%).

Note that we performed similar analyses dividing the sample in two clay content classes (clay content lower or higher than 45%). The corresponding boxplot is shown in Figure 5-22. The Kruskal-Wallis test provides p values <0.001 for dry bulk density and saturated hydraulic conductivity but p=0.018 for near saturated hydraulic conductivity at -20 mm. This result highlights expected and unexpected results: dry bulk density of soils with the highest clay content is the largest as expected. Near saturated hydraulic conductivity of soils with the largest clay content are the lowest as expected also. On the other hand, soils with the highest clay content have also the largest saturated hydraulic conductivity, which is unexpected, but can be understood as we underlined in section 3 that soils with high clay content were generally covered with forests in our sample.

Combining classes derived for dry bulk density and hydraulic conductivity, we are able to build three classes for which retention and hydraulic conductivity curves can be built.
- DB1-KS1: land uses 20, 21, 22 (broad leaf and coniferous forest with moors and fallow)
- DB1-KS2: land uses 11, 12: natural and catered pasture
- DB2-KS2: land uses 10, 20: cultivated pasture and vineyard.

Table 5-8: Parameters of the representative retention curves and hydraulic conductivity curves for the three DB-KS classes

	DB1-KS1 (forest)	DB1-KS2 (natural pasture)	DB2-KS2 (cultivated land)
n	20.9	20.9	20.9
η	25.25	25.25	25.25
h_g (mm)	-67.8	-75.5	-75.5
θs (-)	0.643	0.643	0.50
K (-20 mm) (mm s^{-1})	0.00244	0.007328	0.00728
K_s (mm s^{-1})	0.0925	0.166	0.166
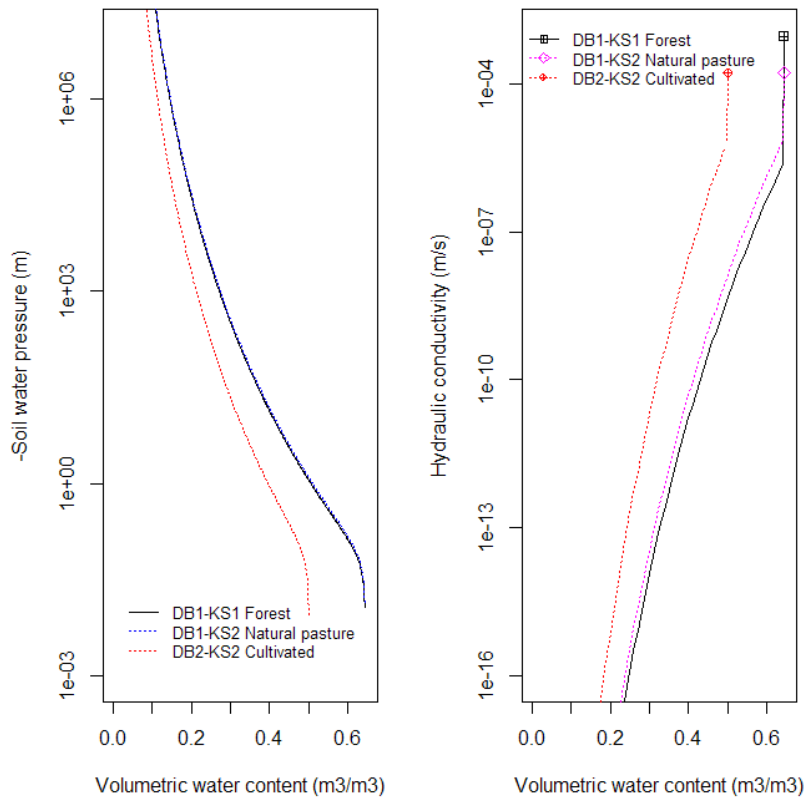
Figure 5-23: Representative retention curves (left) and hydraulic conductivity curves (right) for the three combined DB and KS classes.

The corresponding curves are shown in Figure 5-23 and the parameters of the curves are provided in Table 5-8. We assumed in this curves that the hydraulic conductivity curve changes at h=-20mm from the traditional Brooks and Corey model towards a linear model (in log scale between near saturation and saturation). This model is able to translate the existence of a jump of hydraulic conductivity close to saturation due to the activation of macropores.

These curves can be used as a first approximation for the spatialization of soil hydraulic properties in the Claduègne catchment.

6. Conclusions

In this report, we describe in details how the field infiltration test campaign was conducted in the Claduègne catchment. We also provide the analysis methods used to exploit the infiltration tests and derive the parameters of the retention and hydraulic conductivity curves.

We compared two methods for *Beerkan* and min-disk estimation: the method proposed by Lassabatère et al. (2006) (L06) and an adaptation of the Differential Linearization (DL) method proposed by Vandervaere et al. (2000b). Although the DL-ST method led to a large number of negative hydraulic conductivity, we showed that, when both methods were providing estimates, the results were consistent between the two methods. We identified systematic differences between the methods. A perspective of development is to study more in depth the impact of the choice of the β=0.6 and Φ=0.75 values in the analysis, values which are discussed by Lassabatère et al. (2009) and Nasta et al. (2012).

Finally we compared the in situ values to representative pedotransfer functions, showing the the RB85 pedotransfer is more representative of the spatial variability of in situ data. However, they are not able to explain satisfactorily the observations. On the other hand, we showed that it was possible to segment the in situ data into two classes for the dry bulk density and hydraulic conductivity respectively. In particular, forested soils are shown to have significantly lower dry bulk density and larger hydraulic conductivity than agricultural soils.

These results were further investigated at the scale of the whole Cévennes-Vivarais region by pooling all the available data in this region (Braud et al., 2016).

7. References

Angulo Jaramillo, R., Gaudet, J.P., Thony, J.L. and Vauclin, M., 1996. Measurement of hydraulic properties and mobile water content of a field soil. Soil Science Society of America Journal, 60: 710-715.

Ankeny, M.D., Ahmed, M., Kaspar, T.C., Horton, R., 1991. Simple field method for determining unsaturated hydraulic conductivity, Soil Sci. Soc. Am. J., 55, 467-470

Bonnet S., 2012. Cartographie des zones potentielles de production ou d'accumulation du ruissellement de surface en région cévenole. Master 2 « Eau et ressources », Université de Montpellier 2, 98 pp.

Braud, I., Ayral, P.-A., Bouvier, C., Branger, F., Delrieu, G., Le Coz, J., Nord, G., Vandervaere, J.-P., Anquetin, S., Adamovic, M., Andrieu, J., Batiot, C., Boudevillain, B., Brunet, P., Carreau, J., Confoland, A., Didon Lescot J.-F., Domergue, J.-M., Douvinet, J., Dramais, G., Freydier, R., Gérard, S., Huza, J., Leblois, E., Le Bourgeois, O., Le Boursicaud, R., Marchand, P., Martin, P., Nottale, L., Patris, N., Renard, B., Seidel, J.-L., Taupin, J.D., Vannier, O., Vincendon, B., Wijbrans, A., 2014. Multi-scale hydrometeorological observation and modelling for flash-flood understanding, Hydrology and Earth System Sciences Discussions, 11, 1871-1945, doi:10.5194/hessd-11-1871-2014.

Braud, I., De Condappa, D., Soria, J., Haverkamp, R., Angulo-Jaramillo, R., Galle, S., Vauclin, M., 2005. Use of scaled forms of the infiltration equation for the estimation of unsaturated soil hydraulic properties (Beerkan method). European Journal of Soil Science, 56: 361-374, doi: 10.1111/j.1365_2389.2004.00660.x.

Braud, I., Desparts, J.F., Ayral, P.A., Bouvier, C., Vandervaere, J.P., 2016. Mapping soil surface hydraulic conductivity in the Cévennes-Vivarais region using infiltration tests conducted with different techniques, J. Hydrology and Hydromechanichs, submitted.

Brooks, R.H., Corey, C.T., 1964. Hydraulic properties of porous media, Hydrol. Paper 3, Colorado State University, Fort Collins

Burdine N.T. 1953. Relative permeability calculations from pore size distribution data. Transactions of the American Institute of Mining, Metallurgical, and Petroleum Engineers, 198, 71-77.

Calianno, M., 2010. Infiltrabilité du sol en fonction de la surface échantillonnée. Mémoire de Master 1 STE, UJF, Grenoble.

Chen Li and Young M. H. (2006). Green-Ampt infiltration model for sloping surfaces. , Water Resour. Res., 42, W07420, doi:10.1029/2005WR004468.

Childs, E.C. and Collis-George, C. 1950. The permeability of porous media. Proceedings of the Royal Society London Series A, 201, 393-405.

Cosby, B.J., Horneberger, G.M., Clapp, R.B. and Ginn, T.R., 1984. A statistical exploration of the relationships of soil moisture characteristics to the physical properties of soils. Water Resources Research, 20(6): 682-690.

Fuentes, C., Vauclin, M., Parlange, J.-Y. & Haverkamp, R. 1998. Soil water conductivity of a fractal soil. In: Fractals in Soil Science (eds P. Baveye, J.Y. Parlange and B. Stewart), pp. 333-340, CRC Press, Boca Raton, Florida.

Gardner, W.R., 1958. Some steady-state solutions of the unsaturated moisture flow equation with application to evaporation from a water table, Soil Science, 85, 228-232.

Gonzalez-Sosa, E., Braud, I., 2009. Measure and spatialization of topsoil hydraulic properties in the Mercier catchment. Contribution to WP1 Hydrological and GIS data collection du projet AVUPUR, Rapport du projet ANR AVuPUR, Cemagref, UR HHLY, Mai 2009, 98pp.

Gonzalez-Sosa, E., Braud, I., Dehotin, J., Lassabatère, L., Angulo-Jaramillo, R., Lagouy, M., Branger, F., Jacqueminet, C., Kermadi, S., Michel, K., 2010. Impact of land use on the hydraulic properties of the topsoil in a small French catchment. Hydrological Processes, 24(17): 2382-2399.

Haverkamp, R., Bouraoui, F., Angulo-Jaramillo, R., Zammit, C. and Delleur, J.W. 1998. Soil properties and moisture movement in the unsaturated zone. In: CRC Groundwater Engineering Handbook (ed. J.W. Delleur), pp. 5.1-5.50, CRC Press, Boca Raton, Florida.

Haverkamp, R., Leij, F.J., Fuentes, C., Sciortino, A. and Ross, P.J., 2005. Soil water retention: I. Introduction of a shape index. Soil Science Society of America Journal, 69: 1881-1890, doi: 10.2136/sssaj2004.0225.

Haverkamp, R., Ross, P.J., Smettem, K.R.J. and Parlange, J.Y., 1994. Three-dimensional analysis of infiltration from the disk infiltrometer 2. Physically based infiltration equation. Water Resources Research, 30(11): 2931-2935.

Lassabatère, L., Angulo-Jaramillo, R., Soria-Ugalde, J.M., Cuenca, R., Braud, I., Haverkamp, R., 2006. Beerkan estimation of soil transfer parameters through infiltration experiments. Soil Science Society of America Journal, 70(2): 521-532.

Lassabatère, L., Angulo-Jaramillo, R., Soria-Ugalde, J.M., Simunek, J., Haverkamp, R., 2009. Numerical evaluation of a set of analytical infiltration equations. Water Resources Research, 45: W12415, doi:10.1029/2009WR007941.

Leij, F.J., Haverkamp, R., Fuentes, C., Zatarain, F., Ross, P.J., 2005. Soil water retention: II. Derivation and application of shape index. Soil Science Society of America Journal, 69: 1891-1901, doi: 10.2136/sssaj2004.0226.

Manus, C., 2007. Analyse de la variabilité de la réponse hydrologique à la variabilité des caractéristiques des sols en région Cévennes-Vivarais. Master 2 Recherche Terre Univers Environnement, spécialité Océan Atmosphère Hydrologie, Institut National Polytechnique de Grenoble, 58 pp.

Manus, C., Anquetin, S., Braud, I., Vandervaere, J.P., Viallet, P., Creutin, J.D., Gaume, E., 2009. A modelling approach to assess the hydrological response of small Mediterranean catchments to the variability of soil characteristics in a context of extreme events. Hydrology and Earth System Sciences, 13: 79-87.

Mualem, Y. 1976. A new model for predicting the hydraulic conductivity of unsaturated porous media. Water Resources Research, 12, 513-522.

Nasta, P., Lassabatere, L., Kandelous, M.M., Simunek, J., Angulo-Jaramillo, R., 2012. Analysis of the Role of Tortuosity and Infiltration Constants in the Beerkan Method. Soil Science Society of America Journal, 76(6): 1999-2005.

Parlange, J.-Y. 1975. On solving the flow equation in unsaturated soils by optimisation: Horizontal infiltration. Soil Science Society of America Proceedings, 39, 415-418.

Perroux, K.M., White, I., 1989. Estimation of unsaturated hydraulic conductivity from field sorptivity measurements. Soil Sci. Soc. Am. J., 53.

Philip, J.R. 1969. Theory of infiltration, Adv. Hydrosci., 5, 215-305.

Philip, J.R. 1991. Hillslope infiltration: Planar slopes. Water Resources Res. 27(1), 109-117.

Rault, J., 2010. Infiltrabilité du sol en fonction de la surface échantillonnée. Mémoire de Master 1 STE, UJF,Grenoble.

Rawls, W.J. and Brakensiek, D.L., 1985. Prediction of soil water properties for hydrologic modeling. In: E.B.a.W. Jones, T.J. eds. (Editor), Watershed Management in the eighties. ASCE, Denver, April 30-May 1,1985, pp. 293-299.

Reynolds, W.D., Elrick, D.E., 1991. Determination of hydraulic conductivity using a tension infiltrometer, Soil Sci. Soc. Am. J;? 54, 1233-1241.

Smettem, K.R.J., Parlange, J.Y., Ross, P.J. and Haverkamp, R., 1994. Three-dimensional analysis of infiltration from the disk infiltrometer 1. A capillary-based theory. Water Resources Research, 30(11): 2491-2495.

Smiles, D.E. and Knight, J.H., 1976. A note on the use of the Philip infiltration equation, Aust. J. Soil Sci., 10, 143-150.

Schwartz, R.C., Evett, S.R., Unger, P.W., 2003. Soil hydraulic properties of cropland compared with reestablished and native grassland. Geoderma, 116(1-2): 47-60.

Vandervaere, J.P., 1995. Caractérisation hydrodynamique du sol in situ par infiltrométrie à disques. Analyse critique des régimes pseudo-permanents, méthodes transitoires et cas des sols encroûtés., Université Joseph Fourier, Grenoble I, Grenoble, France, 9 Octobre 1995, 329 pp.

Vandervaere, J.P., Vauclin, M., Elrick, D.E., 2000a. Transient flow from tension infiltrometers: I. The two-parameter equation. Soil Science Society of America Journal, 64: 1263-1272.

Vandervaere, J.P., Vauclin, M., Elrick, D.E., 2000b. Transient flow from tension infiltrometers: I. The two-parameter equation. Soil Science Society of America Journal, 64: 1263-1272.

van Genuchten, M.T. 1980. A closed-form equation for predicting the hydraulic conductivity of unsaturated soils. Soil Science Society of America Journal, 44, 892-898.

Vereecken H. ., Maes, Feyen, J. 1989. Estimating the soil moisture retention characteristics from texture, bulk densit, and carbon content. Soil; Sci. 148:1-12

Vereecken H., Maes, Feyen, J. 1990. Estimating unsaturated hydraulic conductivity from easily measured soil properties. Soil. Sci. 149, 1-12.

Warrick, A. W., and P. Broadbridge (1992), Sorptivity and Macroscopic Capillary Length Relationships, Water Resour. Res., 28(2), 427–431.

Weynants, M., Vereecken H., Javaux, M. 2009. Revisiting Vereecken pedotransfert functions: Introducing a closed-form hydraulic model. Vadose Zone Journal. Vol.8, No.1. 86-95.

White, I. and Sully, M.J., 1987. Macroscopic and microscopic capillary length and time scales from field infiltration. Water Resources Research, 23(8): 1514-1522.

Wooding, R.A., 1968. Steady infiltration form a shallow circular pond, Water Resources Research, 4, 1259-1273.

Yilmaz, K.K., Gupta, H.V., Wagener, T., 2008. A process-based diagnostic approach to model evaluation: Application to the NWS distributed hydrologic model. Water Resources Research, 44(9): W09417.

Zhang, R. 1997. Determination of soil sorptivity and hydraulic conductivity from the disk infiltrometer. Soil. Sci. Soc. Am. J., Vol, 61. July-August. 1031-1036.

8. Appendix 1: complementary results about statistical analysis of the *Beerkan* infiltration tests

Table A 1 : Results of the equality of variance, mean and median for the estimated dry bulk density amongst soil cartographic units. The value in the table is the p.value of the statistical test in the range [0,1]. If p<0.05 (resp. 0.1), then the equality of variance/mean/distribution is rejected at the 5% (resp. 10%) level. The corresponding cells are underlined in grey and blue respectively. When the equality of variance was rejected, the t.test was replaced by a Welch-modified test (see documentation of the t.test function, R software)

UC		26	27	29	33	64	65
8	Variance	0.03	0.99	0.38	0.88	0.04	0.78
	Mean	0.55	0.01	0.0001	0.00	0.04	0.0006
	Distribution	0.60	0.01	0.0006	0.00	0.02	0.0007
26	Variance		0.05	0.13	0.04	0.81	0.10
	Mean		0.54	0.03	0.02	0.05	0.03
	Distribution		0.68	0.01	0.004	0.12	0.02
27	Variance			0.44	0.89	0.07	0.81
	Mean			0.00	0.00	0.005	0.00
	Distribution			0.0001	0.00	0.002	0.001
29	Variance				0.47	0.19	0.63
	Mean				0.26	0.87	1.00
	Distribution				0.35	0.63	0.87
33	Variance					0.06	0.89
	Mean					0.43	0.27
	Distribution					0.33	0.22
64	Variance						0.14
	Mean						0.87
	Distribution						0.94

Table A 2 : Results of the Tuckey HSD test for dry bulk density when UC is considered as the discriminant factor. We underline in blue (resp. in grey) grey the p value (last column) where difference in mean is significant at the 5% (resp. 10% level)

UC combination	diff	lwr	upr	p
65-33	7.20E-02	-0.18871384	0.3327481	0.9776525
29-33	7.21E-02	-0.15524187	0.2993581	0.9561901
64-33	9.06E-02	-0.17010498	0.351357	0.9329065
8-33	3.71E-01	0.13779741	0.6042071	0.000238
26-33	4.52E-01	0.17609153	0.727955	0.0001478
27-33	5.36E-01	0.28643909	0.7850521	0.0000007
29-65	4.10E-05	-0.25542214	0.2555041	1
64-65	1.86E-02	-0.2670076	0.3042253	0.9999938
8-65	2.99E-01	0.03825419	0.5597161	0.0153342
26-65	3.80E-01	0.08044905	0.6795632	0.0052598
27-65	4.64E-01	0.18850154	0.7389554	0.0000919
64-29	1.86E-02	-0.23689526	0.274031	0.9999881
8-29	2.99E-01	0.07164418	0.5262441	0.0034323
26-29	3.80E-01	0.10900557	0.6509247	0.0015134

27-29	4.64E-01	0.21989554	0.7074794	0.0000098
8-64	2.80E-01	0.01964532	0.5411073	0.0276979
26-64	3.61E-01	0.06184019	0.6609543	0.009156
27-64	4.45E-01	0.16989267	0.7203465	0.0001825
26-8	8.10E-02	-0.19491074	0.3569527	0.9697304

Table A 3 : Results of the equality of variance, mean and median for the estimated dry density amongst land use classes. The value in the table is the p.value of the statistical test in the range [0,1]. If p<0.05 (resp. 0.1), then the equality of variance/mean/distribution is rejected at the 5% (resp. 10%) level. The corresponding cells are underlined in grey and blue respectively. When the equality of variance was rejected, the t.test was replaced by a Welch-modified test (see documentation of the t.test function, R software). Land use classes are defined in **Erreur ! Source du renvoi introuvable.**

Land use class		11	12	20	21	22	30
10	Variance	0.45	0.19	0.75	0.72	0.68	0.17
	Mean	0.004	0.02	0.00	0.001	0.001	0.14
	Distribution	0.002	0.01	0.00	0.004	0.0007	0.13
11	Variance		0.66	0.64	0.47	0.78	0.68
	Mean		0.74	0.17	0.08	0.75	0.0007
	Distribution		0.70	0.15	0.09	0.82	0.001
12	Variance			0.33	0.33	0.48	0.94
	Mean			0.13	0.06	0.53	0.004
	Distribution			0.12	0.09	0.82	0.009
20	Variance				0.62	0.89	0.31
	Mean				0.45	0.24	0.00
	Distribution				0.57	0.31	0.00
21	Variance					0.57	0.34
	Mean					0.11	0.00
	Distribution					0.26	0.01
22	Variance						0.48
	Mean						0.0002
	Distribution						0.001

Table A 4: Results of the Tuckey HSD test for dry bulk density when land use is considered as the discriminant factor. We underline in blue (resp. in grey) grey the p value (last column) where difference in mean is significant at the 5% (resp. 10% level)

Landuse combination	diff	lwr	upr	p
20-21	0.05208023	-0.25995028	0.3641107	0.9985037
22-21	0.14067318	-0.19450135	0.4758477	0.8506343
11-21	0.16870944	-0.16646509	0.503884	0.711754
12-21	0.20367279	-0.13150174	0.5388473	0.5068148
10-21	0.45933973	0.15336865	0.7653108	0.0005799
30-21	0.5753992	0.25939363	0.8914048	0.0000227

22-20	0.08859295	-0.15618391	0.3333698	0.9196358
11-20	0.11662921	-0.12814765	0.3614061	0.7604749
12-20	0.15159256	-0.0931843	0.3963694	0.4840227
10-20	0.4072595	0.20430125	0.6102178	0.0000033
30-20	0.52331897	0.30552716	0.7411108	0.0000001
11-22	0.02803626	-0.24563259	0.3017051	0.99991
12-22	0.06299961	-0.21066924	0.3366685	0.9912867
22-22	0.31866655	0.08166237	0.5556707	0.002612
30-22	0.43472602	0.18490168	0.6845504	0.0000522
12-11	0.03496335	-0.2387055	0.3086322	0.9996746
10-11	0.29063029	0.05362611	0.5276345	0.0076858
30-11	0.40668976	0.15686542	0.6565141	0.000164
10-12	0.25566694	0.01866276	0.4926711	0.0269472

Table A 5: Results of the equality of variance, mean and median for the estimated logarithm of saturated hydraulic conductivity amongst soil cartographic units. The value in the table is the p.value of the statistical test in the range [0,1]. If p<0.05 (resp. 0.1), then the equality of variance/mean/distribution is rejected at the 5% (resp. 10%) level. The corresponding cells are underlined in grey and blue respectively. When the equality of variance was rejected, the t.test was replaced by a Welch-modified test (see documentation of the t.test function, R software)

UC		26	27	29	33	64	65
8	Variance	0.03	0.29	0.19	0.44	0.01	0.04
	Mean	0.17	0.03	0.37	0.09	0.21	0.10
	Distribution	0.17	0.02	0.37	0.18	0.43	0.24
26	Variance		0.21	0.21	0.07	0.98	0.63
	Mean		0.48	0.22	0.11	0.56	0.48
	Distribution		0.78	0.27	0.02	0.57	0.26
27	Variance			0.85	0.68	0.15	0.33
	Mean			0.15	0.004	0.96	0.95
	Distribution			0.20	0.003	1.00	0.93
29	Variance				0.49	0.14	0.35
	Mean				0.05	0.38	0.28
	Distribution				0.12	0.53	0.29
33	Variance					0.03	0.10
	Mean					0.09	0.03
	Distribution					0.13	0.04
64	Variance						0.57
	Mean						0.94
	Distribution						1.00

Table A 6 : Results of the equality of variance, mean and median for the estimated logarithm of saturated hydraulic conductivity amongst land use classes. The value in the table is the p.value of the statistical test in the range [0,1]. If p<0.05 (resp. 0.1), then the equality of variance/mean/median is rejected at the 5% (resp. 10%) level. The corresponding cells are underlined in grey and blue respectively. When the equality of variance was rejected, the t.test was replaced by a Welch-modified test (see documentation of the t.test function, R software). Land use classes are defined in **Erreur ! Source du renvoi introuvable.**

Land use class		11	12	20	21	22	30
10	Variance	0.19	0.11	0.36	0.91	0.26	0.33
	Mean	0.50	0.02	0.13	0.17	0.14	0.96
	Distribution	0.85	0.04	0.10	0.18	0.22	0.75
11	Variance		0.63	0.60	0.40	0.96	0.75
	Mean		0.0008	0.24	0.26	0.26	0.45
	Distribution		0.004	0.18	0.14	0.25	0.82
12	Variance			0.33	0.26	0.62	0.44
	Mean			0.00	0.11	0.0004	0.005
	Distribution			0.001	0.09	0.007	0.05
20	Variance				0.58	0.66	0.85
	Mean				0.40	0.96	0.08
	Distribution				0.40	0.72	0.08
21	Variance					0.44	0.53
	Mean					0.39	0.20
	Distribution					0.57	0.07
22	Variance						0.79
	Mean						0.09
	Distribution						0.12

9. Appendix 2 : comparison of the DL and L06 method for the *Beerkan* infiltration tests

The comparison of the results of the DL and L06 methods on the whole sample of *Beerkan* infiltration tests is presented in Figure A 1 and Table A 1provides the statistics of the parameters for the two methods. Note the large proportion of samples leading to negative values of hydraulic conductivity.

Table A 7 : Statistics of the results of the L06 and DL methods on the mini-disk infiltration tests. Negative values were discarded from the analysis.

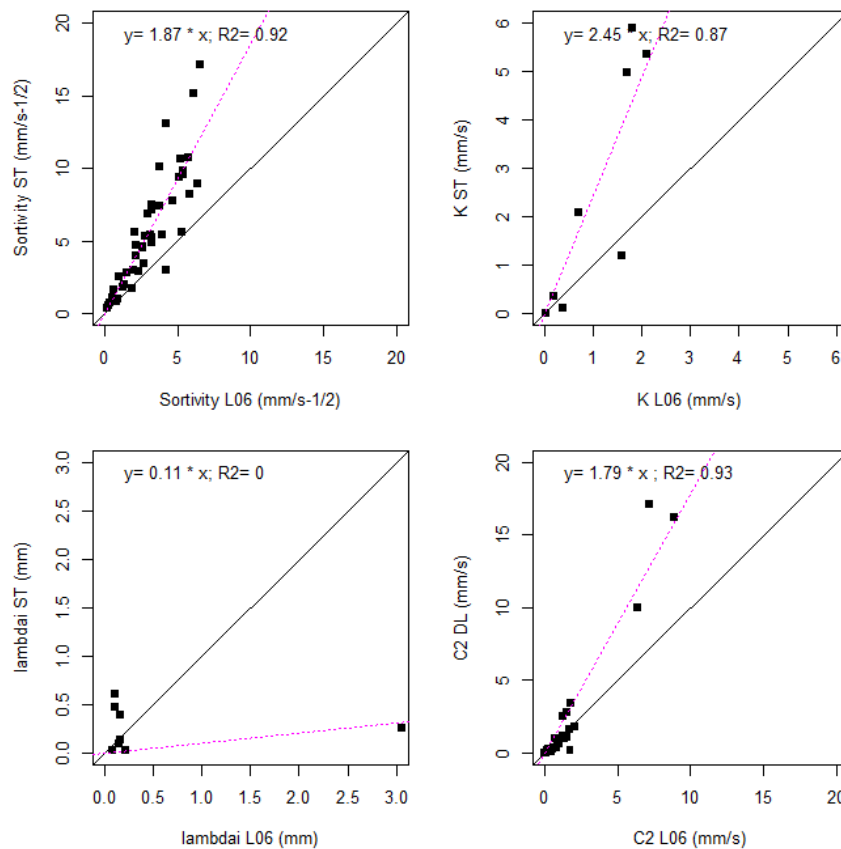|	Mean	Minimum	Maximum	Median	Standard deviation	CV	Nbre points
$C_1 = S$ L06 method	2.84	0.16	6.59	3.02	1.86	0.65	44
$C_1 = S$ DL method	5.59	0.435	17.15	7.89	4.04	0.72	44
$C2$ L06 method	1.09	0.002	8.88	0.39	1.86	1.70	44
$C2$ DL method	1.52	0.002	17.06	0.26	3.72	2.45	44
K L06 method	0.95	0.0237	2.11	0.70	0.85	0.89	9
K DL method	2.23	0.01	5.90	1.20	2.49	1.12	9

Figure A 1 : Comparison of the DL and L06 method for the Beerkan infiltration tests. We show the comparison of $S=C_1$ (top left), K (top right), λ (bottom left) and C_2 (bottom right)

10. Appendix 3 : formula used in the pedotransfer function

Rawls and Brackensieck (1985)

Function type **f** , with C = clay (%) S = sand (%) ϕ = porosity (m³.m⁻³)	$c_1 + c_2.C + c_3.S + c_4.\phi + c_5.C^2 + c_6.C.\phi + c_7.S^2 + c_8.S.\phi + c_9.\phi^2 + c_{10}.C.\phi^2 + c_{11}.C^2.S + c_{12}.C^2.\phi + c_{13}.C.S^2 + c_{14}.C^2.\phi^2 + c_{15}.S^2.\phi + c_{16}.C^2.S^2 + c_{17}.S^2.\phi^2$

	exp (**f**)	exp (**f**)	(**f**)	exp (**f**)
Coefficient	h_{bc}	λ	θ_r	K_s
Unit	cm	-	m³ m⁻³	m
c_1	5.3396738	- 0.7842831	-0.01824820	-8.968470
c_2	0.1845038	0	0.00513488	-0.028212
c_3	0	0.0177544	0.00087269	0
c_4	- 2.48394546	-1.0624980	0.02939286	19.53480
c_5	0.00213853	- 0.00273493	-0.00015395	-0.0094125
c_6	- 0.61745089	0	0	0
c_7	0	-0.00005304	0	0.00018107
c_8	- 0.04356349	-0.03088295	-0.00108270	0.077718
c_9	0	1.11134946	0	-8.395215
c_{10}	0.50028060	-0.00674491	-0.00235940	0
c_{11}	0.00000540	0	0	-0.0000035
c_{12}	0.00895359	0.00798746	0.00030703	0.0273300
c_{13}	- 0.00001282	-0.00000235	0	0.0000173
c_{14}	- 0.00855375	-0.00610522	-0.00018233	-0.0194920
c_{15}	- 0.00072472	0	0	0.0014340
c_{16}	0	0	0	0
c_{17}	0.00143598	0.00026587	0	-0.00298

Cosby et al. (1984)

Function type **f** , with C = clay (%) S = sand (%) Si = silt (%)	$c_1 + c_2.C + c_3.S + c_4.Si$

	10^**f**	1/**f**	**f**	10^**f**
Coefficient	h_{bc}	λ	θ_s	K_s
Unit	cm	-	%	in h^{-1}
c_1	1.54	3.1	50.5	-0.6
c_2	0	0.157	-0.0337	-0.0064
c_3	-0.0095	-0.003	-0.142	0.0126
c_4	0.0063	0	0	0

Weynants et al. (2009). In the formula, clay and sand contents are in %, dry bulk density in g cm^{-3} and organic carbon content in 100 g g^{-1}.

Parameter†	Variable	Coefficient	Value	CI	t statistic	P value
θ_s	intercept	a_2	0.6355	0.0219	56.9679	<0.0001
	clay	b_2	0.0013	0.0002	11.5132	<0.0001
	bulk density	c_2	−0.1631	0.0140	−22.8826	<0.0001
$\alpha^* = \ln(\alpha)$	intercept	a_3	−4.3003	0.1596	−52.8332	<0.0001
	clay	b_3	−0.0097	0.0063	−3.0132	0.0026
	sand	c_3	0.0138	0.0018	14.8296	<0.0001
	organic C	e_3	−0.0992	0.0257	−7.5635	<0.0001
$n^* = \ln(n-1)$	intercept	a_4	−1.0846	0.0625	−33.9996	<0.0001
	clay	b_4	−0.0236	0.0022	−21.2222	<0.0001
	sand	c_4	−0.0085	0.0016	−10.3062	<0.0001
	sand^2	d_4	0.0001	0.0000	17.4583	<0.0001
$K^* = \ln(K_o)$	intercept	a_5	1.9582	0.7543	5.0891	<0.0001
	sand	c_5	0.0308	0.0039	15.5281	<0.0001
	bulk density	d_5	−0.6142	0.4769	−2.5247	0.0116
	organic C	e_5	−0.1566	0.0718	−4.2766	<0.0001
λ	intercept	a_6	−1.8642	0.4536	−8.0567	<0.0001
	clay	b_6	−0.1317	0.0231	−11.1891	<0.0001
	sand	c_6	0.0067	0.0044	2.9822	0.0029

† θ_r, residual water content (m^3 m^{-3}); θ_s, saturated water content (m^3 m^{-3}); K_o, conductivity acting as a matching point at 0 potential (cm d^{-1}); α (cm^{-1}), n, and λ, shape parameters.